Structural and Geologic Mapping of Southern Tellus Regio, Venus: Implications for Crustal Plateau Formation

A Thesis

SUBMITTED TO THE FACULTY OF

UNIVERSITY OF MINNESOTA

BY

Melanie Graupner

(B.Sc. University of Mississippi)

IN PARTIAL FULFILLMENT OF THE REQUIREMENTS

FOR THE DEGREE OF

MASTER OF SCIENCE

Vicki Hansen

January 2013

ACKNOWLEDGEMENTS

To my parents and grandparents

for their

constant support and love

Abstract

Crustal plateau formation on Venus is subject to animated debate. Crustal plateaus are quasi-circular, flat-topped plateaus with heights ranging 1-4 km. These crustal plateaus are host to distinctive tectonic terrain, referred to as ribbon tessera terrain. The debate on crustal plateau formation centers on plateau support and resulting surface deformation. Detailed mapping of southern Tellus Regio, one of two isolated crustal plateaus, provides critical clues for plateau evolution. Southern Tellus Regio records broadly synchronous formation of contractional and extensional structures, accompanied by deposition of flood material. Continuous deformation and deposition of flood material lead to an increase in layer thickness, resulting in the formation of progressively longer-wavelength structures. Short-wavelength folds occur across the entire plateau, the extent of which has previously been undocumented. Early-formed structures and flood deposit material are carried 'piggyback' by later-formed, longer-wavelength structures, recording a complex surface deformation. Generally the early-formed structures (short-wavelength folds and ribbons) record a high structural fluidity, marked by variable orientation of structures or juxtaposition of neighboring structural suites. This structural fluidity later on ceased due to the increase in layer thickness and increase in strength of the layer. This interpretation of the geologic history of the region indicates the necessity of an extremely high geothermal gradient over a huge area and provides a means to evaluate the different crustal plateau hypotheses. The mantle downwelling, mantle upwelling, and pulsating continents hypotheses fail to accommodate the surface features recorded in this study. However, the lava pond hypothesis, in association with the bolide impact hypothesis, provides a suitable hypothesis of crustal plateau formation that accommodates structural elements recorded in this study.

TABLE OF CONTENTS

LIST OF TABLES

LIST OF ILLUSTRATIONS

Supplementary Files

1. INTRODUCTION

Crustal plateaus are one of the major surface features found on Venus, they are subcontinent-sized (1500- 2500 km in diameter), quasi-circular, flat-topped, steep-sided features that sit 1 to 4 km above the surrounding lowlands, which are supported by either thickened crust, or by low-density material in the upper mantle (e.g., Bindschadler et al., 1992; Grimm, 1994; Phillips and Hansen 1994). Crustal plateaus are considered to have formed in the past and record geodynamic processes no longer active today (Basilevsky et al., 1995; Phillips and Hansen, 1994). Venus' five prominent crustal plateaus each host complex deformed surface topography characterized by so-called 'tessera terrain', which is defined by intersecting tectonic lineaments (Barsukov et al., 1986; Basilevsky, 1986). The formation of crustal plateaus remains a topic of dispute, focusing on the formation of this distinct surface terrain, including the size, shape, and ultimately the mechanism by which the plateau is elevated.

The formation of crustal plateaus is subject of animated debate with hypotheses ranging from a global stratigraphy model to specific hypotheses, which each call for a genetic relationship between development of the plateau topography and the deformation responsible for tessera terrain formation (Grimm, 1994; Basilevsky and Head, 1995; Tanaka et al., 1995). The global stratigraphy hypothesis aims to describe the global surface evolution of Venus as a whole, but it has implications for crustal plateau formation, although it is not specifically aimed at the formation of crustal plateaus. Within the global stratigraphy model global deformation of the surface occurs prior to, and unrelated to, later uplift in local regions, forming crustal plateaus. However, the correlation between crustal plateau topography and surface deformation strongly suggests that plateau uplift and the formation of tectonic fabrics are genetically related (e.g., Bindschadler and Head, 1991; Bindschadler, 1995; Hansen and Willis, 1996, 1998; Ghent and Hansen, 1999).

Four hypotheses specifically address the evolution of crustal plateaus as a geomorphic feature: mantle downwelling, mantle upwelling, pulsating continents, and the lava pond

hypothesis. Each of these hypotheses addresses the deformation and topographic evolution and ultimately the uplift of the crustal plateaus by different mechanisms. The mantle downwelling (Bindschadler and Parmentier, 1990; Bindschadler et al., 1992, Bindschadler, 1995), mantle upwelling (Herrick and Phillips, 1992; Phillips and Hansen, 1998; Hansen and Willis, 1998), and pulsating continents hypotheses (Romeo and Turcotte, 2008) call on thickened crust to support the plateau topography, whereas the lava pond hypothesis (Hansen, 2006) calls for low-density mantle melt residuum in the upper-most mantle as a means of isostatic support for the plateau. The three hypotheses that call for crustal thickening postulate different mechanisms to account for crustal thickening, and therefore each hypothesis may make different predictions about the geologic history of the surface during plateau formation. Mantle downwelling calls for crustal thickening and accretion by convective downflow within the mantle or sinking of cold, dense lithosphere (Bindschadler and Parmentier, 1990; Bindschadler et al., 1992, Bindschadler, 1995). The mantle upwelling hypothesis calls for a rising mantle plume creating partial melting in the upper mantle and thickening of the crust by magmatic underplating (Herrick and Phillips, 1992; Phillips and Hansen, 1998; Hansen and Willis, 1998). The pulsating continents hypothesis postulates that periodic subduction events and cyclic compression thicken the crust, forming crustal plateaus (Romeo and Turcotte, 2008). In the case of the lava pond hypothesis the surface deformation and uplift are decoupled, but genetically related. The surface evolves as the result of the progressive solidification of a huge lava pond, with tessera terrain forming the lava pond 'scum'; a related hypothesis calls for the formation of the vast quantity of lava due to massive partial melting in the mantle caused by the impact of a bolide (bolide impact hypothesis); escape of melt to the surface forms the lava pond, whereas topographic support results from low density mantle melt residuum left behind in the mantle (Hansen, 2006). In this case the surface evolves at one timescale, whereas plateau uplift occurs at another, later and slower, timeframe.

All four hypotheses propose different deformation patterns and surface histories that might be recorded on the crustal plateau surface. The mantle downwelling hypothesis calls on

convective down flow, leading to crustal shortening and dominantly contractional structures throughout plateau formation and uplift, followed by later extensional structures formed during collapse; late flooding would be unrelated to plateau formation (Bindschadler and Parmentier, 1990; Bindschadler et al., 1992, Bindschadler, 1995). This hypothesis records early contractional structures and late radial extensional structures of the surface of the plateau. The mantle upwelling hypothesis calls for a rising mantle plume, creating early extensional surface strain throughout uplift of the terrain, with overlapping, but later shortening (Herrick and Phillips, 1992; Phillips and Hansen, 1998; Hansen and Willis, 1998). As a result, this hypothesis would generate a crustal plateau surface dominated by extensional structures, recording early formation of extensional structural elements accompanied by massive basalt flows and generally later formation of folds across the crustal plateau surface; flooding could occur through the surface history. The pulsating continents hypothesis calls for a cyclic compression following a global subduction event, recording early contractional structures, and late stage extensional structures accompanied by late stage deposition of flood material (Romeo and Turcotte, 2008). The lava pond hypothesis calls on solidification of a huge lava pond over time, resulting in the formation of both extensional and contractional structures across a skin or scum that forms across the pond surface; deformation is driven by convection within the lava pond; liquid pond material can leak to the surface through the deformation; the pond scum layer increases in thickness with time and cooling of the lava pond (Hansen, 2006). The crustal plateau surface generated in this hypothesis would record extensional and contractional structural occurring broadly synchronous, accompanied by deposition of flood material over time, and would show an increase in structural wavelengths over time (due to progressive thickening of the pond surface).

Tellus Regio, one of five crustal plateaus and one of only two isolated plateaus, provides an excellent opportunity to examine the rich surface deformation history, which was preserved during crustal plateau formation, enabling the evaluation of crustal plateaus hypothesis. Tellus Regio sits in the northern hemisphere of Venus. The northern portion of the plateau is not well

defined in comparison to the western, eastern and southern margins, which are all surrounded by lowlands along a sharp topographic gradient. Southern Tellus Regio has been the subject of several focused studies, aimed at describing the distribution of features, the timing between volcanism and deformation (Banks, 2000; Banks and Hansen, 2000), and the evolution of southwestern Tellus and other local regions (Gilmore and Head, 1995, 1996; Straley and Gilmore, 2007; Gilmore, 2009; Gilmore et al., 2010, 2011); however, a geologic map of southern Tellus Regio, which would provide regional context of the area, has not yet been published.

This study of southern Tellus Regio investigates the surface evolution of southern Tellus Regio in order to better understand: 1) the spatial distribution of structural elements across the southern portion of the plateau, 2) the relative timing for contractional and extensional structural features and deposition of flood material, and 3) implications for crustal plateau formation. This study provides new observations and detailed geologic histories for the entire region and is in concordance with some of the previous geologic mapping of the area. The geologic elements and spatial and temporal relations are similar across southern Tellus Regio, recording formation of abundant early short-wavelength folds and orthogonal ribbon structures, followed by the formation of intermediate-wavelength folds and later long-wavelength folds, and the formation of graben complexes. Deformation occurs broadly synchronously with flood material deposition. The previously undocumented extent of short-wavelength folds and orthogonal ribbons preserve a record of high structural fluidity of a surface layer, recording variable structural orientations and strain patterns, whereas later structures display more coherent patterns. A general increase in layer thickness is necessary to form progressive structural wavelengths. The documented geologic history and implications for surface evolution require a high geothermal gradient, with a sharp decrease in viscosity at depth between deforming surface layer and subsurface material, as previously documented for part of Ovda Regio (Hansen, 2006).

The observations and implications of this study can be used to evaluate crustal plateau formation hypotheses. The mantle upwelling hypothesis, mantle downwelling hypothesis and the

pulsating continent hypothesis are difficult to reconcile with the geologic evolution of southern Tellus Regio as reported herein. The lava pond hypothesis provides a mechanism that not only depicts the surface evolution as recorded on southern Tellus Regio, but also provides supporting evidence to explain the arising implications.

2. BACKGROUND

The evolution of crustal plateaus is focused on several models that are quite different. Global stratigraphy is a hypothesis that aims to describe global surface evolution which has implications for crustal plateaus, but is not aimed at their formation. Four hypotheses describe the evolution of crustal plateaus as a geomorphic feature. All four hypotheses aim to address the deformation and topographic evolution of crustal plateaus. A few localized studies describe the surface evolution specific to Tellus Regio. In this section I give a short description of global stratigraphy and then discuss the four formation hypothesis for crustal plateaus in more detail. The local studies of Tellus Regio will be discussed in the following section.

2.1 CRUSTAL PLATEAU HYPOTHESES

Global stratigraphy is a hypothesis that concerns itself with the evolution of the Venusian surface (Basilevsky and Head, 1998). This hypothesis has implications for crustal plateau formation but is not intended to specifically address the formation of crustal plateaus. Global stratigraphy begins with intense tectonic deformation of the global surface forming ribbon tessera terrain (RTT), which is later locally uplifted to form crustal plateaus; subsequently low areas are flooded resulting in burial of low lying RTT. The global stratigraphy hypothesis predicts that crustal plateau deformational patterns would be unrelated to the uplift of the crustal plateau. Therefore, the deformation of the surface has no spatial relation to plateau topography. However, the correlation between crustal plateau topography and surface deformation strongly suggests that plateau uplift and the formation of tectonic fabrics are genetically related (e.g., Bindschadler and

Head, 1991; Bindschadler, 1995; Hansen and Willis, 1996, 1998; Ghent and Hansen, 1999), thus the global stratigraphy hypothesis is not considered further herein.

Four hypotheses address the formation and evolution of crustal plateaus as a class of geomorphic features. Plate 1 and Figure 1 give an overview of theses hypotheses including structural features and evolution of crustal plateaus. All four hypotheses discuss a genetic relationship between deformation and elevated topography. Mantle downwelling calls for crustal thickening due to lower crustal flow (Bindschadler and Parmentier, 1990; Bindschadler et al., 1992, Bindschadler, 1995). The mantle upwelling hypothesis calls on a mantle plume rising to shallow depths causing massive partial melting which leads to magmatic underplating (Phillips and Hansen, 1998; Hansen and Phillips, 1998; Hansen and Willis, 1998). The pulsating continents hypothesis involves cyclic subduction events that lead to thickening of the crust by tectonic compression and lateral accretion (Romeo and Turcotte, 2008). The lava pond hypothesis uses progressive deformation and solidification of the surface 'scum' of a huge lava pond to explain the formation of crustal plateaus. In this hypothesis topographic support results from buoyant mantle melt residuum (Hansen, 2006).

The mantle downwelling hypothesis (Plate 1A and Figure 1A) begins with globally thin crust or lithosphere above a ductile mantle. Convective down-flow in the mantle and/or sinking of cold, dense lithosphere leads to sinking of the crust. The evolution of the model begins with a downward flexed surface, which accretes the crust by continued downward flow of the ductile lower crust. During this process, contractional features start to form in the upper crust, generating a ring of elevated topography around the affected area. In the later stages of the model, the center of the thickened crust spreads under its own weight and creates extensional features in a radial pattern across the plateau. The spatial distribution and size of individual crustal plateaus depend on the size of the area that experienced the initial downwelling. The mantle downwelling hypothesis calls for deformation resulting from crustal shortening, with localized extensional collapse of highly thickened regions, resulting in a high ratio of contractional and extensional

6

structures in the center of the crustal plateau and contractional structures dominating along the plateau margins. Extensional structures postdate contractional structures.

The mantle upwelling model (Plate 1B and Figure 1B) also begins with an initially globally thin lithosphere. A mantle plume rises from the core-mantle boundary causing extensive partial melting in the upper mantle. The overlying crust is heated and mechanically annealed, erasing all previous structures and leaving a thin, brittle membrane over a ductile substrate behind. Internal convection of hot mantle melt underneath the thin crust leads to an increase in tensile stresses and to the uplift of the terrain. Extension of the thin, brittle crust over the ductile substrate allows for the formation of ribbon terrain across the expansion of the individual plateau follows. Locally, melt seeps to the surface causing massive basalt flows. As the plume evolves the crust thickens by magmatic underplating, increasing the brittle-ductile-transition (BDT) depth. Cooling and subsidence lead to local shortening, causing the formation of folds. During the late stages crustal relaxation and local collapse cause local extension normal to fold crests resulting in graben formation. Tensional stresses caused by the upwelling of the plume result in extensional features, which are spatially constrained by the initial upwelling surface. Localized areas of contraction form after the initial extensional period and are distributed over the crustal plateau. Extensional ribbon structures should dominantly predate intermediate and long-wavelength folds.

The pulsating continents hypothesis (Plate 1C and Figure 1C) initiates with a low density crust analogous to continental crust, which is underlain by relatively thick lithosphere that survived postulated global subduction. Eclogite formation in the lower crust causes sinking and results in crustal shortening and thickening accompanied by formation of concentric thrust faults. Contraction ends when an equilibrium between density forces is reached and the plateau rises due to isostatic adjustment resulting from the thickened crust. Throughout this process a gravitational instability within the cold lithospheric mantle develops and begins sinking, leading to formation of radial extensional features along the plateau margin. Throughout the same process the crust is thickened by the sinking of cold mantle material. Radial extensional widens the areal extent of the

plateau, accompanied by contractional features at the boundary of the evolving plateau and the surrounding plains. Decompression during the late stage of the pulsating continents model creates local partial melting and surface flooding of structural lows. During deformation and thickening, the crust becomes decoupled from the mantle lithosphere and permits the initiation of the next, so-called, global subduction event. The size of an individual crustal plateau is similar to the initial continental crustal region. Volcanism and flooding occur at all stages of the evolution after initial crustal contraction. Overall, the crustal plateau created by this process is dominated by concentric thrust faults and folds.

The lava pond hypothesis (Plate 1D and Figure 1D), associated with the bolide hypothesis, begins with a large bolide piercing a globally thin lithosphere, and causes massive partial melting in the upper mantle; the melt rises to the surface, forming a huge lava pond, which will ultimately evolve into the surface of the crustal plateau. The lava pond solidifies and forms 'scum', representing the tessera terrain; whereas the mantle-melt residuum ultimately leads to plateau uplift. The lava pond surface scum is deformed by convection in the pond; the surface experiences both contraction and extension, with early formed short-wavelength folds and extensional ribbon structures normal to fold crests. Melt locally leaks to the surface filling local lows. Scum layer thickening occurs over time due to continued deformation, progressive cooling, deposition of flood material and solidification in structural lows. The increase in layer thickness of the lava pond scum leads to progressive increase in structural wavelengths of both extensional and contractional features. The mantle from which the melt was extracted is host to an expanse of mantle melt residuum with lower density compared to the surrounding mantle. Isostatic adjustment in the mantle ultimately results in uplift, raising the solidified pond on the surface. The lava pond and bolide hypothesis considers two end-member results. 1) Because the mantle-melt residuum resides in ductile mantle it could be stripped away by mantle convection, resulting in collapse of the associated crustal plateau. 2) Conversely, if the lithosphere thickens due to secular cooling, the residuum will remain in place and retain the crustal plateau at its elevation.

8

The spatial extent of the crustal plateau depends on the size of the lava pond, which relates to the initial bolide impact event.

These four hypotheses consider the general formation and evolution of crustal plateaus, including the deformation history and how the crustal plateau becomes uplifted. Each model shows different final structural deformation patterns, which can be compared and evaluated with geologically and structurally mapped crustal plateaus. Other models consider solely the surface deformation and "structural events" to explain the features recorded. Detailed information of surface deformation models for Tellus Regio will be provided in the next section.

2.2 TELLUS REGIO

Tellus Regio, commonly referred to as Tellus Tessera, is one of five prominent crustal plateaus on Venus. Tellus Regio, centered at 42.6°N 76.8°E, is nearly oval with a slightly smaller and tapered southern part, has a long axis dimension of ~2300 km (International Astronomical Union), is bordered by lowlands, and sits 2-3 km above the regional plains with the highest elevations in the eastern, western, southern portions, and steep eastern and western margins and gently sloping northern and southern margins (Bindschadler et al., 1992; Senske, 2010). The northern margin of Tellus Regio is not well defined and may represent a transitional area to the lowlands. The northern boundary is the topic of study by Aaron Slonecker (Slonecker and Hansen, 2012). North-central Tellus is host to a low-lying plateau interior showing complex surface deformation (Bindschadler and Tatsumura, 1992). High-resolution synthetic-aperture-radar data reveals an overall rough surface topography on Tellus Regio marked by ribbon tessera terrain.

Tellus Regio, one of only two isolated crustal plateaus on Venus, shows areas that are dominated by variable structural patterns, although distinct domain boundaries are not clearly identifiable. The eastern and western margins of southern Tellus Regio are bounded by long-wavelength folds (25 to 150 km) with crests parallel to the plateau margins and lengths up to 750

km (Plate 2). Folds dominate the southern margin with NE-trending crests cut by fold-crest-orthogonal graben. Much of the interior of southern Tellus Regio appears as radar-bright surfaces, indicating rough surface topography, although several radar-dark basins are distinguishable throughout the plateau. The interior shows apparently complex deformation created by structures such as multiple wavelength folds, ribbons, and graben. Structural lows associated with a wide range of structures are filled by low viscosity flood material (most likely by lava fill), forming basins of variable sizes and shapes (commonly elongated). The majority of large basins (e.g. ~90-125 km long axes) occur along the boundaries and within the southern portion of the plateau, whereas smaller basins (~50 km long axes) are distributed throughout the interior.

2.2.1 Previous Tellus Regio Studies

Tellus Regio has been the subject of various studies over the past 20 years. Construction of the 1:5 million scale geologic map of Tellus Regio (V10), is assigned to D. Senske and J. Plaut, but is not yet published (http://astrogeology.usgs.gov/PlanetaryMapping/MapStatus/VenusStatus/Venus_Status.html). Tellus Regio has also been topic of several focus geologic studies, although most of these studies are only published as abstracts (Banks and Hansen, 2000 is the one exception). Focus geologic studies include: a comparison study between Tellus Regio and Phoebe Regio focused on the variability of tessera terrain across Venus (Senske, 2010); analysis of northern Tellus Regio aimed at an interpretation of the make-up of crustal plateau terrain and implications for stratigraphy (Senske and Plaut, 2009); analysis of the overall age and distribution of large wavelength structures within Tellus Regio (Bindschadler and Tatsumura, 1992; Gilmore and Head, 1995); detailed geologic mapping of so called intra-tessera basins and adjacent regions with the goal to understand the timing between volcanism and deformation at Tellus Regio (Banks, 2000 (M.S. thesis); Banks and Hansen 2000); and several geologic studies focused on

constraining the evolution of southwestern Tellus Regio (Gilmore and Head, 1996; Straley and Gilmore, 2007; Gilmore, 2009; Gilmore et al., 2010, 2011).

Senske (2010) compared the tessera terrain of Tellus Regio and Phoebe Regio; and they suggested that Tellus Regio is composed of layered rock units and small tessera provinces that collided to form the majority of tessera terrain. In comparison, he suggested that Phoebe Regio displays a gradational contact with the regional plains and that it records surface deformation within a dominantly extensional tectonic environment.

Senske and Plaut (2009) interpreted that parts of Tellus Regio are composed of thick layered volcanic sequences that were deformed to create tessera terrain; they further suggested that uplift and deformation resulted in exposures similar to plateau basalts of the Columbia River Plateau on Earth.

The distribution of large scale features on Tellus Regio have been mapped and interpreted within the context of different studies (Bindschadler and Tatsumura, 1992; Gilmore and Head, 1995). Linear to arcuate ridges, segmented by troughs (later defined as ribbons, see Hansen and Willis, 1996, 1998) and graben, are interpreted as evidence for early crustal contraction, with late stage deformation dominated by extension and local volcanism. These workers postulate that contractional structures and late-stage deposition of flood material coincide with mantle downwelling.

Detailed geologic mapping of intratessera basins illustrates the complex temporal relations between volcanism and deformation at Tellus Regio (Banks, 2000; Banks and Hansen, 2000). These workers suggest that volcanic flooding of structures at all wavelengths implies that volcanism and tessera terrain deformation occurred roughly at the same time, and that there was a progressive increase in fold wavelength formation with time (from <1km to up to 150 km). The early formation of ribbon structures and early flooding of ribbon troughs is interpreted as evidence of an early high geothermal gradient during the evolution of Tellus Regio, with a

decrease in thermal gradient with time—taken collectively as support for the mantle upwelling hypothesis.

Gilmore and coworkers examined southwest Tellus Regio and divided the region into several tectonic provinces including: an indenter, fold belt, crustal plateau interior, and NE and SE marginal zones (Gilmore and Head 1995, 1996, Straley and Gilmore, 2007; Gilmore, 2009; Gilmore et al., 2010, 2011). The indenter, a strong block postulated to have collided with other parts of Tellus, is interpreted to affect the structures within Tellus Regio's interior. A ridge belt divides the indenter and interior, echoing the shape of the indenter. These workers suggested that mean fold wavelengths within the indenter are ~13 km (intermediate wavelengths), and that shorter-wavelength folds (8 km) occur within other zones. Gilmore and others suggested that the crustal plateau interior behaved in a ductile fashion and responded to a collision with the rigid indenter; they further proposed that the folds developed on a crust with a ductile substrate, bounded on top by a brittle surface. Their modeling also implied that folds at these wavelengths formed by deformation of a layered crust comprised of an upper brittle crustal layer (thickness of 2-5 km) overlying a ductile crustal substrate. These workers suggest that Tellus Tessera terrain formed during a single mantle downwelling event.

In summary, several different workers appear to agree that during the development of tessera terrain at Tellus Regio: the surface layer thickness increased with time, that deformation and volcanism occurred throughout plateau evolution, and that the regional geothermal gradient decreased over time (Gilmore and Head 1995, 1996, Banks, 2000; Banks and Hansen, 2000; Straley and Gilmore, 2007; Gilmore, 2009; Gilmore et al., 2010, 2011). These conclusions have implications for the interpretation of the evolution of structures in relation to crustal plateau formation hypothesis. The previous studies disagree on the character of the initial thermal gradient (i.e. average gradient with late cooling, or high gradient with late cooling), the details of the rheological structure, and the evolution of the rheological structure, of the surface layer across Tellus Regio.

3. DATA SETS AND MAPPING METHODOLOGY

3.1. DATA

Tellus Regio is one of the areas on Venus covered by all three NASA Magellan mission synthetic-aperture-radar (SAR) mapping cycles, providing a large range of data coverage over the study area, which can be utilized for geologic mapping. The NASA Magellan Mission collected gravity, emissivity, altimetry, and SAR data across the surface of Venus. Gravity and emissivity data is beyond the scope of this project. Altimetry and SAR data covering the same area will be used to create a geologic map of the study area (Ford and Plaut, 1993). Altimetry and SAR data sets can then be used to create true and synthetic stereo imagery that aids in interpretation of structural elements.

The Altimetry and SAR data sets, both of which were obtained at different resolutions, provide broad and detailed information on surface topography. The altimeter measured the distance between the spacecraft and the surface of Venus (Plaut, 1993). The data was collected at points on a grid spaced 20 km by 8 km; altimetry resolution varies with spacecraft altitude (10-30 km horizontal resolution). Two different types of altimetry data are available. The altimetry-radiometry Composite Data Record shows data in table format and the Global Data Record is in map format (Plaut, 1993). Altimetry data highlights the transitional zones between the crustal plateau and lowlands, but its resolution is too coarse to provide detailed information on the surface topography of structures within Tellus Regio. The SAR data provides information on the surface topography and surface roughness that is not recorded by altimetry data. The side-looking radar penetrates the thick Venusian cloud cover with pulses of microwave energy at a wavelength of 12.6 cm, with a resolution of ~100 m/pixel (Ford et al., 1993). Three mapping cycles (1, 2, and 3) varied the look-direction and the incidence angle, which is the angle between the radar beam and the vertical normal to the surface. The incidence angle is key in the determination of brightness and radar imagery tones (Farr, 1993). Cycle 1 mapped 83.7% of the surface at an

13

average resolution of ~300 m. During this cycle, left-look data (SAR pointed east) was collected with incidence angles ranging from 35.8° to 42.1° over the study area on southern Tellus Regio. Cycle 2 was dedicated to filling data gaps of cycle 1. The incidence angle during cycle 2 was much lower and collected both right- and left-look radar images. Cycle 3 acquired left-look coverage, using the same flight path but different incidence angles (Ford et al., 1993).

Altimetry and SAR data sets are used to create synthetic and true stereo images that allow the interpretation of longer-wavelength structures. SAR and altimetry data can be combined to create synthetic stereo (Kirk et al., 1992) using a macro created by Duncan Young. The process of creating synthetic stereo involves digital enhancement, the creation of a simulated image using altimetry and SAR data, which are combined, rendered by a computer to provide oblique perspective views that can be arranged to create synthetic stereo pairs that can be viewed digitally as red-blue anaglyphs. The resolution of synthetic stereo is lower than true stereo, but proves useful for large areas and areas where true stereo is unobtainable. True stereo images, similar to stereo (aerial) photographs are created by overlapping two SAR images with different incidence angles depicting the same area (Plaut, 1993). Cycle 3 data provides images suitable for the creation of a stereo pair with cycle 1 data; stereo images are viewed as red-blue anaglyphs through which the relief of the terrain becomes three-dimensional.

True stereo images have a higher resolution than synthetic stereo and depict the topography more precisely, although in neither case is topography quantified. Given that true stereo data is available for the majority of the study area I used these images.

3.2. INTERPRETATION OF SAR DATA

NASA Magellan SAR data provides a means to view the surface of southern Tellus Regio allowing an interpretation of structural elements. SAR images are created when a radar beam leaves the spacecraft, aimed to the surface, and then reflecting back to the spacecraft. SAR waves are scattered once they reach the surface of Venus, smooth surfaces scatter the incoming

waves in a specular direction, almost mirror-like, with little energy returning to the spacecraft, and thus such areas appear radar-dark. Rougher surfaces scatter the signal in a more random fashion, therefore returning more energy to the spacecraft SAR antenna, and thus rough areas appear radar-bright (Farr, 1993). Ultimately this leads to lighter tones for rough terrain and darker tones for smooth terrain. The orientation of structures relative to spacecraft and look-direction is also important, because different sides of a terrain will be highlighted. Several different types of structures and features are recognizable including folds, faults, fractures, graben, wrinkle ridges, volcanic features and impact craters (Stofan et al., 1993; Weitz, 1993; Ford et al.1993; Senske and Stofan, 1993; 1993; Tanaka et al, 2010).

SAR data provides valuable information on the surface topography but throughout the interpretation issues may arise. All radar interpretation has to be completed with caution. Factors such as topographic relief artifacts can distort the image and the interpretation. Depending on the backscatter, slopes may be appear shortened or elongated (foreshortening or elongation). Radar shadow, which occurs when a slope facing away from the view direction is larger than the incidence angle (Conners, 1995), will prohibit an image record and appear as a dark shadow. Layover, foreshortening, and elongation are amplified at low incidence angles, whereas radar shadow is amplified at large incidence angles (Tanaka et al., 2010). For the latitudes at which Tellus Regio is located, layover, elongation, and foreshortening will be slightly increased, while radar shadow is decreased. The use of both left-look and right-look radar data can alleviate or even eliminate possible data gaps due to radar shadow. Spatial resolution, depending on slant range, size and the distance from the detector to the target (Zimbelman, 1999) can influence the produced radar image. Any features below the identification resolution cannot be included in any examination and therefore even smaller scale structural features are yet to be determined. For a detailed discussion of radar artifacts see Ford et al. (1993).

Altimetry, SAR, synthetic stereo, and true stereo can be digitally enhanced and mapped for the features and structures found. Given the digital nature of the data, the radar images can be

enhanced to a certain degree. Photoshop™ grants the option of "stretching" the images, and inverting the left-look and right-look radar images, which can enhance the visibility of specific structural features. Inverted left-look and right-look SAR is a valuable tool to interpret structural elements, providing more look-directions and highlighting structural elements, which are hard to distinguish in regular, un-inverted SAR. True and synthetic stereo improve the discernability of long-wavelength features and aid in geologic mapping. Adobe Illustrator™ enabled the mapping of southern Tellus Regio's geology on left- and right-look SAR, inverted images, and true stereo images.

3.3. GEOLOGIC FEATURES AND STRUCTURAL ELEMENTS

SAR images provide information with respect to surface character and geomorphology, which can, in turn, be interpreted as material units or specific structural elements. Furthermore, SAR images reveal information on areas and linear patterns (lineaments) using surface roughness and shape of the terrain. Areas and linear patterns can then, based on their character, be interpreted as specific structures. This section discusses material units, lineaments and the interpretation of geologic features from these two types of terrain.

3.3.1. Material units

Surface roughness reveals the characteristics and extend of a certain terrain (areas), but does not highlight much information on morphological features. Areas, commonly interpreted as material units, are highlighted by radar backscatter and are typically highlighted by surface roughness which may show a range of dark tones. Large areas, or material units, are commonly interpreted as volcanic features, lava flows and burial of structural lows (basins) and occur broadly across the surface of southern Tellus Regio. Their presence implies that low viscosity melt seeped to the surface and embayed preexisting structures. Surface melt on Venus has a lower viscosity than on Earth due to a coupling between radiative and convective heat transfer between atmosphere and melt, allowing individual flows to travel further distances than on Earth (Snyder,

16

2002). Because of this low viscosity, large outlines of radar smooth surfaces can provide information on structural and topographic control, much like water on Earth (Ford et al., 1993). The lava surface marks a horizontal plane across extensive regions where lava fill occurs within troughs of structural elements. As the terrain gets more deformed over time, this record remains, providing evidence of an earlier paleohorizonal plane, which was later deformed.

3.3.2. Lineaments

Geomorphic features (lineaments) and structures are interpreted using the different surface characteristics displayed by radar imagery. Lineaments mark lines (no topographic expression), ridges, or troughs; each of these can represent different structures depending on their character. Tones of linear features can vary, showing either gradual changes in tones (ridges or troughs marked by gradual slope changes) or abrupt changes (marking sharp topographic slope changes). Lineament character can be highly variable, ranging from straight, to sinuous, to anastomosing. Lineaments can occur in pairs, in which two lines of similar length run parallel to each other. Suites of lineaments appear with different wavelengths, pertaining to the spacing from crest to crest (or from trough to trough). Extensional features commonly appear in fairly straight lines, whereas contractional features generally show more variable sinuosity.

Lineaments can be ridges, crests, or troughs depending on their character. Ridges, separated by troughs, are lineaments with sharp boundaries, in which the illuminated direction shows a dark lineament followed by a white lineament. Crests are lineaments in which the tones show a gradational boundary relative to change in topographic slope, and are widely identified as elevated topography. The direction of radar illumination relative to the orientation of the trough influences the discernability of the structures. Structures oriented parallel to look direction are typically harder to identify, although using SAR images with different look directions can allow for a better identification.

3.3.3. Structures

In this section the characteristics and identification of structural features are discussed. Figure 2 shows radar imagery and geologic mapping of most of the types of structural features found on Tellus Regio. Figure 2 depicts tessera terrain dominated by short- and intermediate-wavelength folds and ribbon structures; identification of lineaments is described below. In addition to SAR, true stereo imagery was used to interpret intermediate-wavelength folds.

Light lineaments, with gradational boundary changes in topographic slope (Figure 2, dark arrows), variable sinuosity (more discernible at a larger scale) and rare chevron-like pattern (in plan view) occur throughout the plateau. The lineaments are marked by parallel topographic ridges and troughs (less apparent), representing fold crests and troughs, respectively (Stofan et al., 1993). Generally, radar brightness grades from darker to lighter tones toward the crest, with a gradual change in slope (Figure 2, dark arrows). Commonly occurring in ridge belts, these lineaments are composed of widely spaced sinuous ridges and interpreted as folds. Suites of folds (alternating smooth ridges and troughs) are generally spaced at different wavelengths, ranging from short- to intermediate- and long-wavelengths (<1 km, 1-5 km, >25km).

Lineaments also appear in pairs, representing ridges separated by troughs that generally display low sinuosity (Figure 2, white arrows). Dark lineaments preceding bright lineaments (in left-look images), are commonly interpreted as ridge-trough bounding surface, in which the structure is facing away from the radar, followed by ridges, where the bright lineament is a ridge-trough bounding surface that faces the radar. Lineament pairs with alternating parallel ridges and troughs commonly appear in suites extending across a large area. Lineaments with these characteristics and a high length-to-width ratio are interpreted as ribbon structures, or ribbons (Figure 2), and are distinguished by their terminations (Hansen and Willis, 1998). Tensile-fracture ribbons show v-shaped terminations, whereas shear-fracture ribbons show parallel terminations, marking a ramp-like termination. Data look-direction affects which side of a ribbon

18

ridge appears radar-bright, the wall facing the radar shows brighter tones than the wall facing away from the radar, which due to its radar-shadow location will show a darker tone. For example, a ribbon ridge facing to the left will appear bright in left-look radar images and dark in right-look images. The use of both left- and right-look SAR data allow for more complete delineation of ribbon structures.

Elongate depressions with suites of parallel lineaments bounding each side, with a low length-to-width aspect ratio, are commonly interpreted as graben, or graben complexes, composed of suites of oppositely-dipping normal faults (e.g. Bindschadler et al., 1992; Stofan et al., 1993; Ghent and Hansen 1998).

Structures found on Venus have different kinematic associations. Folds and wrinkle ridges are widely interpreted as contractional structures, whereas suites of ribbon structures, fault scarps, and graben are generally interpreted as extensional structures. Troughs are geomorphic features, and as such troughs can be part of either folds or ribbon structures (or even channel features) and are generally not interpreted as a contractional or extensional features (e.g., Basilevsky, 1986; Bindschadler and Parmentier, 1990; Phillips and Hansen, 1996, 1998; Hansen and Willis 1998).

Crustal plateaus are characterized by the occurrence of tessera terrain; the formation of tessera terrain is intimately linked with the formation of crustal plateaus, and records a surface history which should provide clues to the geologic history of individual crustal plateaus and as geomorphic features recording geodynamic processes (Hansen and Willis, 1998). The term tessera was first used for complex deformed terrain, which is the intersection of two or more structural features. Tessera terrain, characterized by high surface roughness, is elevated in relation to surrounding region, and thus shows up as radar-bright regions in SAR (Basilevsky et al., 1986). Tessera terrain fabric is not uniform across individual crustal plateaus but consists of a combination of folds (multiple wavelengths), ribbons, troughs, graben and buried regions (Hansen and Willis, 1996). Commonly tessera terrain hosts ribbons and graben oriented

orthogonal to fold crests (Hansen and Willis, 1996, 1998). Multiple wavelengths of structures commonly trend along a similar orientation. Troughs and structural lows with lava fill occur throughout the terrain. Together, all of these features and structures record a rich deformational history.

3.4. RELATIVE TIMING

Tellus Regio is host to a variety of structures with different spatial and temporal relations that allow the interpretation of a geologic history. Relative temporal relations between structures aid in the understanding of how the plateau surface evolved over time. The interpreted relative timing between structural elements, and the interpreted process by which individual structural elements formed can be intertwined (Hansen and Willis, 1998; Hansen, 2006), and one seeks a coherent, internally consistent scenario to relate suites of structures. Spacing and geometric relationships with respect to other suites of structures can place important constraints on the relation and temporal evolution of these suites (e.g. 3D architecture through time). In this section I outline some general guidelines for the identification of temporal relationships between suites of structures, with specific attention to southern Tellus Regio.

The relative timing of flood material (by lava fill) of local structural topographic lows can provide clues about the relative timing between different structural elements, and the relative timing of structural element formation and the evolution of the surface topography. The formation of several suites of structural elements within southern Tellus results in characteristic surface topography or morphology. Flood material can result in the burial of local topographic lows. Flood unit material emplaced within local structural topographic lows may cover all or portions of earlier formed structures. The flood unit material could provide a new surface that could in turn host later-formed (young) structures, or record evidence for the reactivation of earlier-formed (old) structural elements. Pre-flood deposit structures can be locally embayed by flood material. Flood material units preserved in topographically elevated local structural troughs may indicate

flood material that predated the formation of the structural element responsible for the local uplift of earlier formed troughs (i.e. prior to elevation of the surface) (Hansen and Willis, 1998; Hansen, 2006).

These relationships collectively record early formation of the locally buried structural elements and later formation of the structural elements linked to local elevation of that surface. Generally, structural elements that cut local fill material are considered younger than the fill material. However, such structures could also represent early-formed structures that were locally buried and experienced reactivation. For example, the deposit material within large intra-tessera basins is host to both wrinkle ridges that post-date fill deposition, and to reactivated structures such as fractures and ribbon structures that formed prior to fill deposition but which experienced reactivation following fill emplacement. The relative timing between single lineaments, such as fault scarps and wrinkle ridges, are commonly discernible due to clear crosscutting relationships.

Several of the detailed map areas within southern Tellus Regio show two or more fold suites with wavelengths ranging from short-, intermediate-, to long-wavelength (Table 1). Fold crests of all wavelength fold suites are generally parallel across each local map area, although local deviations occur. Short-wavelength folds typically occur along crests, limbs, and troughs of intermediate- and long-wavelength folds. In the portions of the fold troughs covered by basin fill, the short-wavelength folds are buried. The relationships noted herein are similar to the relationships documented on northern Ovda Regio by Hansen (2006). The presence of flood unit material within shorter-wavelength fold troughs that reside on the crests and limbs of longer-wavelength folds indicates that the longer-wavelength folds carried shorter-wavelength folds and their buried lows 'piggyback', and records progressive formation of folds and respective burial from early-formed short- to later-formed long-wavelength folds as documented in northern Ovda Regio (Hansen, 2006), see Hansen for further discussion of these temporal relations. Short-wavelength folds regularly occur within the broad topographic ridges created by intermediate- or long-wavelength fold crests. Intermediate-wavelength folds also occur on the troughs, limbs, and

crests of long-wavelength folds. Local flood material of the structural lows marked by fold troughs also provides important evidence for the temporal relationships between different fold suites, as defined by wavelength. If flood material deposition occurred during or after folding, then local topographic lows should be filled covering previously formed structures. The presence of flood material within short-wavelength fold troughs that are preserved within the broad topographic ridges marked by the crests of long-wavelength folds indicates that the flood material of the short-wavelength fold troughs occurred before the formation of the long-wavelength folds. Similar relations argue for the formation of short-wavelength folds with respect to intermediate-wavelength folds. If all flood material had occurred late with respect to folding (i.e. after all fold formation), then there should be no basin fill within the short-and intermediate-wavelength fold troughs that are preserved at high elevations. In this case, flood deposits should only occur within the long-wavelength fold troughs. Similarly, if short-, intermediate-, and long-wavelength folds formed at the same time, and flood material occurred after such a synchronous fold formation events, only the troughs of long-wavelength folds should be buried (Hansen, 2006). Therefore the fact that short- and intermediate-wavelength fold troughs that reside on the limb and crest of long-wavelength folds are locally filled by flood material collectively indicate that progressive deformation of multiple-wavelength folds (early short-wavelength folds and late long-wavelength folds) was accompanied by local burial of structural lows through time and evolution.

Shear-fracture ribbon structures, extensional features marked by suites of oppositely dipping normal-faults, could either postdate or predate fold formation (Hansen and Willis, 1998). Both scenarios would show an apparent bend in ribbon structure lineaments along fold crests of folds due to radar foreshortening artifacts (Hansen and Willis, 1996). The formation of ribbon structures and the relative temporal relations of ribbon structures and folds are complex subjects and have previously been discussed in depth (Hansen and Willis, 1998; Hansen, 2006). Herein I present a brief overview of the temporal relations of ribbon structures drawn from previous studies, with examples from southern Tellus Regio. The formation of ribbon structures requires a

thin upper layer and a high geothermal gradient, similar to the formation of short-wavelength folds (Gilmore et al., 1998; Ghent and Tibulaec, 2002; Ruiz, 2007). These relationships indicate that both families of structures–ribbons and short-wavelength folds–could form with a broad overlap in time; further interpretation of timing might be gleaned from crosscutting relationships.

Ribbon formation requires a shallow depth to the BDT, in order to form steep to near-vertical trough walls and narrowly spaced ribbons over a large area (Hansen and Willis, 1998; Hansen, 2006). If intermediate- and long-wavelength folds had predated the ribbon- structure formation, then the support for intermediate- and long-wavelength folds would require a fairly deep BDT (Hansen and Willis, 1998). Thus late formation of periodic ribbon structures would require a dissection of a thick and strong brittle layer, presumably by periodically-spaced high-angle faults. However, the periodic spacing of ribbon structures is inconsistent with deformation of a thick layer. However, if ribbon structure formation predated the formation of intermediate- and long-wavelength folds, then the BDT could increase in depth with time, allowing an early shallow BDT during the formation of ribbons, followed by a deeper BDT during the formation of intermediate- and long-wavelength folds. Therefore it is likely that ribbon structure formation predated the formation of intermediate- and long-wavelength folds.

Crosscutting relationships involving graben complexes provide clear relative temporal constraints within other structural elements with ribbon tessera terrain (e.g. Bindschadler, 1992; Ghent and Hansen, 1999; Hansen and Willis, 1998; Banks, 2000; Banks and Hansen, 2002; Hansen, 2006; Gilmore et.al, 2010 and 2011). Graben complexes, composed of east- and west-facing scarps in southern Tellus Regio, display wider-trough regions than ribbon structures; the scarps typically truncate fold crests and troughs providing clear temporal relations. Graben-complex formation coincided with, or was followed by, deposition of low viscosity flood material within the graben-complex trough, generally burying earlier formed structures.

4. GEOLOGIC MAPPING OF SOUTHERN TELLUS REGIO

Geologic mapping provides insight into the geologic history of Tellus Regio. Observations about the type of structures present and their spatial and temporal relationships allow for the interpretation of the evolution of the plateau surface. Geologic mapping was conducted in Adobe Illustrator [TM], using full resolution Magellan SAR imagery, with the tools described in the previous section. In this chapter I describe geologic mapping results, for Tellus Regio and six detailed map areas (Figure 3), selected for their characteristic structural elements and their distribution across the plateau. This section will follow a similar path than the geologic mapping process. The introduction and detailed description of southern Tellus Regio will be discussed, followed by descriptions and relative timing for all six windows. The histories and implications derived for each window are subsequently discussed in the regional context of southern Tellus Regio.

4.1. SOUTHERN TELLUS REGIO MAP AREA

This section discusses the geologic mapping of southern Tellus Regio. Mapping was completed on two separate regions, each mapped in using left-and right-look SAR imagery; the regions were spliced together in order to interpret the plateau as one region. True stereo SAR images were used in order to note changes in topography and distributions of structures across areas. The regional southern Tellus Regio geologic map illustrates the locations and orientations of intermediate-and long wavelength fold crests and troughs, ribbon trends, graben complexes, and intratessera-basins. Preliminary mapping established that short-wavelength folds and ribbon structures are too small and far too abundant to illustrate the scale of this map. Therefore, only ribbon structure trends are shown, and short-wavelength folds are not included in this regional map. Portions of short-wavelength folds and ribbon structures are shown in window maps.

Tellus Regio, located in the north-central hemisphere of Venus, is a crustal plateau rising 2-3 km above mean-planetary radius. Tellus Regio is near-oval shaped with a tapered southern

end with bordering lowlands to all sides (Plate 2). The plateau is characterized by tessera terrain, a distinctive surface deformation defined by the interaction of two or more structures (strongly deformed) and basins that together define a fluid pattern. The lowlands surrounding Tellus Regio are host to few types of structural and/or volcanic elements, including wrinkle ridges, double lineaments, shields and pit chains.

Within the plateau, tessera terrain includes various combinations of long-, intermediate-, and short-wavelength folds, intra-tessera basins, ribbon structures, graben complexes, fault scarps, and undefined lineaments. Long- wavelengths folds dominate the plateau generally occurring along the margins of Tellus Regio, although a few long, NW-trending wavelength folds occur in the center of the plateau. Intratessera basins are broadly distributed across the plateau, and occur at a range of sizes, shapes and orientations. Large intratessera basins are widely distributed across the plateau and commonly represent fill of long-wavelength fold troughs. Intermediate-wavelength folds occur across the plateau defining a general fluid pattern. Relatively broad elongate embayments also form in the troughs of intermediate-wavelength folds. Along the crest of long-and intermediate-wavelength folds short, narrow basins occur in structural troughs of short-wavelength fold and ribbon structures. Ribbon structures occur across the plateau. Graben complexes generally appear in suites throughout the central and western region of southern Tellus Regio. Fewer graben complexes occur in the eastern portion of the plateau.

The consistent distribution of structural elements collectively defines a fluid-like pattern across the entire plateau surface. Four impact craters are located in the southern and eastern portion of southern Tellus Regio.

Southern Tellus Regio is host to several suites of characteristic structures: long-, intermediate-and short-wavelength folds, ribbons, graben complexes, and faults scarps, undefined lineaments, and wrinkle ridges, which deform basin, fill material. Plate 2 shows dominant structures, but due to the resolution of the data, short-wavelength folds, undefined lineaments and

fault scarps are not depicted. Long -and intermediate -wavelength folds, ribbon structures and graben show different orientation, wavelengths, and inter-structural relations. The geologic map of southern Tellus Regio highlights structural patterns across the map area (Plate 3). For descriptive purposes the map area is divided into five areas; central, south-central, western and eastern margins and south-west (Plate 3a). These areas do not represent structural or geologic domains, but are used here simply for descriptive purposes.

Long-and intermediate-wavelength folds dominate southern Tellus Regio. Long wavelength folds which occur along the eastern margin and within the south-western portion of southern Tellus Regio generally trend NE with wavelengths > 25 km. Suites of long-wavelength folds in the central and south-central area trend NW and show slight curvature in the northwestern most point (Plate 3c). Abundant intermediate-wavelength folds, which generally parallel long-wavelength fold trends, trend NE in the southern area, NW in the central and western area and NNE in the eastern area of southern Tellus Regio. Along the western margin, intermediate-wavelength folds show the highest variability in trend. Where present, short-wavelength folds generally parallel long- and intermediate-wavelength fold trends, and exist along the limbs and crests of long-and intermediate-wavelength folds. Suites of ribbons generally trend normal to fold crests.

Southern Tellus Regio is also host to several levels of basin fill within structural basins. Units, fb_{c1} and fb_{c2}, are dispersed throughout the area, showing two different stages of flood material. Basins, forming in the troughs of intermediate- and long-wavelength folds, dominate the southern, eastern and western areas. A region in the central map area lacks major flood deposits. The northern area represents the topographically lowest region in the southern Tellus Regio map area (Figure 4); here major basin fill covers the troughs of various structural elements. Finger-like flood material fill (units fb_a and fb_b) in the troughs of short- and wavelength folds are too detailed to be depicted on the regional map. Wrinkle ridges that cut basin fill material generally trend SW and show change in trend further north. Four impact craters occur with the eastern and

southern areas. NE-trending pit chains occur along the southeastern margin of the map area and cut across previously deposited structures.

The map area includes several suites of extensional features. Ribbon structures trend NE in the southeastern and south-central areas, and trend NW in the central area (Plate 3d). These ribbons generally show little variability in their trend within a suite. In the south-western area, ribbon structures generally parallel long-wavelength fold crests, whereas in other regions ribbon generally trend orthogonal to the fold crests. Suites of graben complexes occur throughout the area, trending NE in the southeastern area and trending NW elsewhere.

In order to better understand the evolution of southern Tellus Regio, six windows across the plateau were selected to be mapped in detailed (Figure 3). The term window in this study refers to detailed geologic maps of areas in southern Tellus Regio, revealing geologic and temporal relations down to the resolution of the data. The following section discusses the detailed geometric and temporal relationships for each of the six windows.

4.2. DETAILED MAPPING

Mapping of the six windows provides an opportunity to examine the detailed geologic and temporal relationships for structural elements across southern Tellus Regio. Each window was selected for characteristic features: window A was selected for its extensive ribbon tessera terrain, composed of dominant intermediate-and short-wavelength folds; window B was chosen based on the presence of intermediate- and short-wavelength fold terrain; window C was selected due to its location along the plateau margin and the preservation of short- and intermediate-wavelength fold terrain; window D was selected for the occurrence of long-wavelength and intermediate-wavelength folds; window E was chosen due to the preservation of ribbon, long- and short-wavelength fold terrain and; window F was selected due to the presence of multiple wavelength folds and basins. These six windows contribute to provide a detailed geologic history

of the crustal plateau. For each window I will present the detailed geologic relations followed by a discussion of relative timing.

4.2.1. Window A - Geologic Relations and Relative timing

Window A (Plate 4) is located in the NE corner of the map area near the lowland transition (Figure 3). It was selected for its extensive ribbon terrain, and dominant intermediate- and short-wavelength folds. This area is dominated by two basins. One basin trends NE and the other trends E-W creating broadly equal regions low deformation (covered basins) and regions of high deformation (inter basinal). Both basins include finger-like embayments that show a preferred E-W trend, mark the troughs of intermediate-wavelength folds; fold crests preserve deformational structures that formed prior to basin burial. Both basins host parallel periodic wrinkle ridges; the NE basin also includes two circular features that are also marked by wrinkle ridges. Inter basin regions, marked by high deformation are host to ribbon structures and short-wavelength folds.

Window A (Plate 4) includes several suites of characteristic structures: intermediate-wavelength folds, short-wavelength folds, ribbons, lineaments, wrinkle ridges and concentric ridges. Each suite shows different orientation, wavelengths, and relations to another. Intermediate-wavelength folds (wavelengths 8-9 km; Table 1) are widely distributed throughout the area with fold crests generally trending W, but locally trending WSW. Short-wavelength folds and ribbons structures are preserved on the limbs and crests of the wavelength folds. Short-wavelength folds crests generally parallel intermediate-wavelength fold crests, with wavelengths ranging from 0.73-0.77 km (Table 1). A suite of narrowly-spaced ribbon structures extends over the majority of the area, generally trending NNW, with trough-to-trough spacing of 1.5-2.3 km (Table 1). Ribbon orientation is nearly orthogonal to adjacent intermediate- and short-wavelength fold crests. The basin fill within intermediate-wavelength fold troughs displays markedly less deformation. Wrinkle ridges, generally spaced 0.85-1.2 km, occur across both large basins, with

W to WSW trends, generally parallel to intermediate-wavelength fold crests. In the north-central portion of the window a set of concentric ridges rises above the basinal plain. Both near-circular structures have a long axis dimension of ~23 km and are defined by wrinkle ridges.

Basin fill deposits and structures cutting across the fill dominate window A. A set of NNW-trending lineaments that parallel ribbon structures extends throughout the NW part of the area. The area also shows different levels of flooded structural lows, ranging from large to small basins and fill within structural lows (most likely by lava fill). The fill of two large basins, unit fb_{c1} in the NE and SW, dominates window A. This basin fill material extends into the contiguous structural lows of intermediate-wavelength troughs. Locally, isolated basins in intermediate-wavelength fold troughs also contain basin fill, and short-wavelength fold troughs and ribbon troughs also show evidence of local burial.

The temporal relations of structural elements in window A (Plate 4) are characteristic of the larger southern Tellus map area. N-trending ribbons cut short-wavelength fold crests and troughs, as evident by a slight offset of fold crests along the ribbon scarps. In addition, short-wavelength folds also terminate along ribbon-trough scarps indicating short-wavelength folds formed before ribbon structures. Ribbon structures are carried piggyback on intermediate-wavelength folds, interpreted due to the increased layer thickness necessary for the formation of intermediate-wavelength folds and the periodicity of ribbon structures present, as discussed in section 3.4. Thus ribbon structures generally postdated the formation of short-wavelength folds and predated the formation of intermediate-wavelength folds. Basin fill occurs within the troughs of both short-wavelength folds and ribbon structures. The fill is marked by fingerlike extensions of radar-smooth terrain into structural lows, indicating that the troughs of both short-wavelength folds and ribbons provided embayment regions for the basin fill, and therefore both families of structures predated the emplacement of this flood material. Intermediate-wavelength fold troughs are also partially buried by flood deposits, covering preexisting structures. Along the crest and limbs of intermediate-wavelength folds, short-wavelength folds and ribbons are preserved.

29

Preservation of these structures and the cover of preexisting structures within intermediate-wavelength fold troughs, together indicate that the burial of intermediate-wavelength fold troughs postdated, or coincided with, the formation of intermediate-wavelength folds. A late stage of burial created the two major basins within window A. The basin fill extends along finger-like embayments into the trough of long-wavelength folds. This basin fill deposition is only postdated by the formation of wrinkle ridges which deform the fill. The two concentric ridges in the northeastern basin are surrounded by basin fill, although not covered, indicating that these ridges likely formed prior to emplacement of the basin fill material.

The relationships between structures that form broadly synchronous (i.e. contractional and extensional structures) enable the interpretation of 2D bulk strain ellipses (Hansen and Willis, 1996 and 1998; Banks and Hansen, 2002; Hansen, 2006). When structures form broadly at the same time, their orientation might be related to the bulk strain; fold crests (and troughs) and wrinkle ridges parallel the direction maximum elongation (x axis), whereas ribbon structures, and graben fault scarps parallel the direction of minimum elongation (z axis) (Figure 5). It is important to note that these structures mark the orientation, but not the magnitudes of bulk principle strain. Interpretations of 2D bulk strain over time are show for each window map area.

In the case of Window A bulk strain orientation does not change through the development of ribbon tessera-related structures, and changes only slight with the formation of wrinkle ridges (Plate 4).

4.2.2. Window B – Geologic relations and Relative Timing

Window B is located in the interior of the map area, and within the center of the plateau (Figure 3). This region was selected for detailed mapping due to the presence of intermediate- and short-wavelength fold terrain. Area B is dominated by intermediate-wavelength folds and their respective finger-like fold-trough basins in the NE and E; extensive short-wavelength folds occur throughout the remainder of the area. Structures that formed prior to basin fill are

preserved across the crests and limbs of intermediate-wavelength folds. The short-wavelength folds in the southern portion of the map show distinct changes in orientation within the same suite of folds. Graben complexes and ribbons occur throughout the SW portion of the window. Short-wavelength folds and ribbons each show variability in trend within this region.

Window B characteristic structures include: intermediate-wavelength folds, short-wavelength folds, ribbons, graben complex and fault scarps (Plate 5), with each suite showing different orientation, wavelengths, and relations to another. Intermediate-wavelength folds (wavelengths 9.3 -11.2 km; Table 1) occur in the NE portion of the window and generally trend NW. Short-wavelength folds with wavelengths of 0.73-1.23 km and ribbons structures with spacing of 2.1-2.67 km (Table 1) are preserved on the limbs and crests of the intermediate-wavelength folds. Short-wavelength fold trends generally parallel intermediate-wavelength folds, although short-wavelength folds show a higher variability in orientation. Suites of narrowly-spaced ribbons within the northern part of the area trend NW, whereas ribbons in the south trend N. Ribbons trend at high angles to all folds. A set of NW-trending graben complexes occur in the southwest portion of the window; whereas fault scarps occur across the window, generally trending parallel to ribbon structures. Basin fill in this window is limited to basins within the troughs of intermediate-wavelength folds (unit fb_b) and basins within short-wavelength fold troughs (unit fb_a). Few isolated basins are present and one graben complex shows fill.

The temporal relations of structural elements in window B (Plate 5) are characteristic of the larger southern Tellus map area. Short-wavelength folds are widely distributed generally showing similar trends, although in the southern portion of the window the trends are highly variable with gradually changes in orientation. Locally, ribbons that trend orthogonal to fold crest cut short-wavelength folds, as evident by offset of fold crests along the ribbon scarps. These relations indicate that short-wavelength fold formation generally predated ribbon formation. Ribbon structures also show changes in trend from the northern to the southern portion of the map area. Basin fill occurs within the troughs of both short-wavelength folds and ribbon structures.

31

The fill is marked by small elongate basins of radar-smooth terrain extending into both types of structural lows. These relationships indicate that both short-wavelength folds and ribbons provided an embayment region for the basin fill, and therefore both families of structures predated the emplacement of the flood material (unit fb_a). Intermediate-wavelength folds are concentrated in the northern portion of the map area and occur locally within the southern region where they show variability in trend. The crests and limbs of intermediate-wavelength folds preserve short-wavelength folds and ribbons. Intermediate-wavelength fold troughs are partially buried by basin fill, covering preexisting structures. Preservation of these structures, and the cover of preexisting structures within intermediate-wavelength fold troughs, together indicate that burial of these intermediate-wavelength fold troughs postdated or coincided with, intermediate-wavelength fold formation. A suite of NW-trending graben complexes cut across all preexisting structures and portions of flood material unit fb_b. Due to the graben complex width the majority of preexisting structures were erased during graben complex formation. These relationships indicate that graben complex formation occurred late during surface evolution. A suite of graben complex-parallel fault scarps also cut across all features. These fault scarps most likely accompanied graben complex formation, or formed shortly after complex formation. Further time constraints prove difficult because these suites of structures are spatially separate.

Geometries and relative timing of structures in window B provide the tools for the interpretation of 2D bulk strain. Early ribbon troughs are generally perpendicular to early short-wavelength fold crests. This relationship supports the interpretation that short-wavelength folds and ribbon structure formation occurred broadly synchronously, and that bulk 2D strain of the (thin) layer during this time is oriented so that short-wavelength fold axes mark the direction of maximum elongation (i.e. principle maximum strain axis x) and perpendicular ribbon troughs parallel the minimum principle strain axis (z) (Hansen and Willis, 1996 and 1998; Banks and Hansen, 2002; Hansen, 2006). Plate 5 depicts the bulk strain change for this window over time. The bulk strain ellipse for intermediate-wavelength fold is similarly oriented to the previous bulk-

strain ellipse; intermediate-wavelength fold crests mark the direction of maximum elongation. During late deformation, as the extensional graben complexes are formed, the bulk strain ellipse for window B is almost opposite to that of earlier bulk strain.

 4.2.3. Window C - Geologic Relations and Relative timing

Window C (Plate 6), located in the NW portion of the regional map area, near the border to the lowland (Figure 3), was selected for detailed mapping due to its location and the preservation of short- and intermediate-wavelength fold terrain. This area consists of two parts, the western and eastern region, dominated by deformation, divided by a central N-trending basin. The central basin shows a tapered shape narrowing to the south, and is host to reactivated structures and wrinkle ridges. The western and eastern regions both depict small, finger-like embayments in the troughs of intermediate-wavelength folds. Along the crests of intermediate-wavelength folds short-wavelength folds are preserved. Graben complexes are prominent throughout the eastern portion of the area; another graben complex occurs in the NW corner of window C. Ribbons occur across the map area and parallel the margins of the central basin. For the purpose of examining this area in depth, the map discussion is divided into the western and eastern regions and the central basin.

The western region includes: intermediate-wavelength folds, short-wavelength folds, ribbons, graben complexes, and fault scarps (Plate 6). Each structural suite shows different orientation, wavelengths, and relations to another. Intermediate-wavelength folds show wavelengths of ~10 km (Table 1), generally trending NW covering the majority of the western portion. Short-wavelength folds generally parallel intermediate-wavelength folds and exist along the limbs and crests of intermediate-wavelength folds. Some short-wavelength folds appear to be covered with a thin veneer. Short-wavelength folds display wavelengths of ~1km or more. Few suites of ribbons occur on the limbs and crests of intermediate-wavelength folds. Two levels of basin fill occur within structural lows; unit fb_a occurs in troughs of short-wavelength folds and

ribbons, and unit fb_b occurs in the troughs of intermediate-wavelength folds. Ribbon structures occur throughout the western region, and along the central basin.

These ribbons generally show little variability in their orientation, trending NE-NNE orthogonal to fold crests. A graben complex and a set of fault scarps trending NW, parallels to the fold crests.

The eastern region includes intermediate-wavelength folds, short-wavelength folds, ribbons, graben complexes, and faults scarps (Plate 6). Two distinct suites of intermediate-wavelength folds show wavelengths of 6-11 km (Table 1), generally trending NNE. Short-wavelength folds generally parallel intermediate-wavelength folds although a few short-wavelength folds trend NW. Some short-wavelength folds appear to be covered with a thin veneer. All short-wavelength folds display wavelengths < 1km. The eastern region has fewer basins. Finger-like basins material unit fb_b are located in the troughs of intermediate- wavelength folds. Basin fill unit fb_a occurs as embayment in troughs of short-wavelength folds and ribbons. A suite of ribbons in the south generally trends NW oriented orthogonal to both intermediate- and short-wavelength fold crests. Another suite of ribbons located on the border to the central basin trends NNE orthogonal to adjacent fold crests. Graben complexes throughout the eastern region trend NW and are oriented orthogonal fold crests, and parallel to fracture ribbons. NW-trending graben complexes are easier to identify in the eastern region than in the western region as a result of the trend of earlier formed structural fabric. In the E region graben complexes trend at a high angle to the penetratively developed NE-trending fold fabric, whereas in the W region graben complexes trend parallel to the penetratively developed NW-trending fold fabric. A set of NW-trending fault scarps cut across eastern region.

The central basin region hosts covered short-wavelength folds wavelengths < 1km, shear fracture ribbons, lineaments and wrinkle ridges (Plate 6). Covered short-wavelength folds generally trend NW, with fold crests exposed from surrounding basin fill material. Unidentified

N-trending lineaments occur in the south, and roughly mirror the eastern border of the basin. The basin itself includes two stages of flood material units fb_{c1} and fb_{c2}.

The temporal relations of structural elements in window C (Plate 6) are characteristic of the larger southern Tellus map area, and provide an important tool to interpret the history of the area. I discuss each region in turn.

In the western region ribbon structures cut short-wavelength folds, indicating that ribbon formation postdated short-wavelength fold formation. Ribbon structures show gradual changes in trend near the central basin. Locally, flood deposits cover the troughs of both short-wavelength folds and ribbon structures, indicating that the short-wavelength folds and the ribbon structures predated emplacement of flood material unit fb_a. Intermediate-wavelength folds, which dominate the eastern region, are host to abundant parallel short-wavelength folds and a few orthogonal ribbon structures. The presence of parallel short-wavelength folds along the limbs and crests of intermediate-wavelength folds suggests progressive formation of multiple-wavelength folds, with short-wavelength fold formation predating intermediate-wavelength fold formation. Ribbon structures are interpreted as predating formation of intermediate-wavelength folds, as discussed in section 3.4. Intermediate-wavelength fold troughs are partially buried by basin fill unit fb_b. Preservation of short-wavelength folds and ribbon structures on fold limbs and crests and the cover of preexisting structures within intermediate-wavelength fold troughs, indicate that burial of intermediate-wavelength fold troughs generally postdated the formation of intermediate-wavelength folds. A NW-trending graben complex located in the northwestern region of window C cuts local structures, indicating that the graben complex formed late.

The eastern region shows similar temporal relationships to the western region, although the orientations of the structural elements are different in the two regions. NW-trending tightly-spaced ribbons cut NE-trending short-wavelength folds, indicating that ribbon formation postdated short-wavelength fold formation. Ribbon structures in the eastern region trend NW, and trend NNE near the central basin. Local flood deposits embay the troughs of both short-

wavelength folds and ribbon structures, providing evidence that both of these families of structures predated the emplacement of unit fb_a. The presence of parallel short-wavelength folds along the limbs of intermediate-wavelength folds suggests progressive formation of multiple-wavelength folds, with early short-wavelength fold formation, and concurrent early ribbon structures formation. As elsewhere, intermediate-wavelength fold troughs are also locally partially buried by basin fill material unit fb_b, indicating that unit fb_b postdated intermediate-wavelength fold formation. The suite of NW-trending graben complexes cut all local structures, indicating that the graben complexes formed late.

The central basin, generally lacking in structural elements, displays a few WNW-trending folds although most of structures are covered by flood deposit material units fb_{c1} and fb_{c2}. The southern part of the basin hosts short-wavelength folds, which are covered by a veneer, indicating that basin fill postdated short-wavelength fold formation. Scarps, locally cut short-wavelength folds and basin fill material. Wrinkle ridges also cut basin fill material.

Window C preserved two regions with near-opposite structural fabric orientations, yet preserving similar temporal relations, and the regions appear to have been juxtaposed commonly, later deforming as a coherent package. The western and eastern regions record early orthogonal ribbons and short-wavelength folds, relations consistent with broadly synchronous, formation and coherent bulk 2D strain (Plate 6) (Hansen and Willis, 1996 and 1998; Banks and Hansen, 2002; Hansen, 2006). The 2D bulk strain ellipses for the western and eastern regions are nearly opposite to one another. The 2D bulk strain associated with intermediate-wavelength fold formation remained unchanged; however, during the formation of the graben complexes both regions experienced maximum elongation strain to the NE.

4.2.4. Window D - Geologic Relations and Relative timing

Window D (Plate 7), located in the south-central map area (Figure 3), was selected due to the occurrence of long-wavelength and intermediate-wavelength folds. Window D is dominated

by long-wavelength folds with flooded trough basins. The window is divided into three regions, NW, central and NE. The central region hosts NW-trending long-wavelength folds and long narrow basins. The limbs and crests of long-wavelength folds structures host previously formed structures. Short-wavelength folds and ribbons are present throughout the area and show variable orientations. The troughs of intermediate- and short-wavelength folds show stages of burial. In the northwestern region graben complexes trend NW. The SW and NE regions host generally parallel short-wavelength folds and ribbon structures.

Window D includes long-, intermediate- and short-wavelength folds, ribbons, graben complexes, fault scarps and wrinkle ridges (Plate 7). Long-wavelength folds (wavelength ~37 km, Table 1) trend NW in the center of the window. Intermediate-wavelength folds (wavelengths ~ 5.9 km) occur on the limbs of long-wavelength fold crests, trending NW and paralleling the long-wavelength folds. Locally, short-wavelength fold crests parallel the intermediate- and long-wavelength fold crests; ribbon structures preserved on the limbs and crests of long-wavelength folds generally trend NE orthogonal to fold crests, similar to geometric relations observed in other map areas. In contrast, the graben complexes and fault scarps trend NW parallel to intermediate-wavelength fold crests. Window D has abundant embayment basins, marking the troughs of long-, intermediate- and short-wavelength folds, and ribbons. Long-wavelength fold troughs display long, narrow and curvy basins filled with unit fb_{c1} unit fb_{c2}. Finger-like embayments mark the troughs of intermediate-wavelength folds filled with unit fb_b and short-wavelength folds and ribbon troughs filled with unit fb_a. Locally, E-trending wrinkle ridges cut fill in the larger basins. The central region includes NW-trending graben complexes. The SW and NE regions host short-wavelength folds (wavelengths from 2-3.5 km) that generally trend NW, and orthogonal ribbons. Throughout the area, fault scarps trend NW.

The temporal relations of structural elements in window D (Plate 7) are characteristic of the larger southern Tellus map area, and provide an important tool to interpret the history of the area. Ribbons structures cut orthogonal-oriented short-wavelength folds in the western and

eastern region, as discussed in section 3.4, indicating that short-wavelength folds predated ribbon

structures, and locally coincided with, ribbon structure formation. Basin fill material covers the

troughs of both short-wavelength folds and ribbon structures, marked by small elongate basins of

radar-smooth terrain extending into both types of structural lows, indicating that the short-

wavelength folds and the ribbons predated the emplacement of unit fba. Intermediate-wavelength

folds are concentrated in the central region of the map area. Along the crest and limbs of

intermediate-wavelength folds short-wavelength folds, ribbons and early basin fill appear

preserved. The presence of parallel short-wavelength folds along the limbs and crests of

intermediate-wavelength folds suggests progressive formation of folds, with short-wavelength

fold formation predating intermediate-wavelength fold formation. Ribbon structures are

interpreted as predating formation of intermediate-wavelength folds, as discussed in section 3.4.

The troughs of intermediate-wavelength folds are partially buried by basin fill unit fb_b.

Preservation of short-wavelength folds and ribbon structures on fold limbs and crests, and the

cover of preexisting structures within intermediate-wavelength fold troughs indicate that burial of

intermediate-wavelength fold troughs generally postdated the formation of intermediate-

wavelength folds. The area is also host to a suite of long-wavelength folds, which trend NW.

Preserved short-and intermediate-wavelength folds, ribbon structures and local basin fill occur on

the limbs and crests of long-wavelength folds. Preservation of preexisting structures on

topographically uplifted regions along long-wavelength fold crests and limbs indicates that the

long-wavelength folds formed after the other structures. Long-wavelength fold troughs are

covered by late flood material units fb_{c1} and fb_{c2} indicating that the fill material was deposited

after the long-wavelength folds formed. Locally partially buried short- and intermediate-

wavelength folds and ribbons predated this stage of basin fill, and may have been partially

reactivated after basin fill emplacement. A suite of NW-trending graben complexes cut across

local structures, including portions of late flood material unit fbc1, indicating graben complexes

formed late.

Geometries and relative timing of structures in window D provide the tools for the interpretation of 2D bulk strain. The three regions preserve different early structural fabric orientations, yet each record similar temporal relations. The regions appear to have been juxtaposed after their early formation and later deformed as a coherent package. The southwestern and northeastern regions each record early orthogonal ribbons and short-wavelength fold relations consistent with broadly synchronous formation and a coherent bulk 2D strain (Plate 7) (Hansen and Willis, 1996 and 1998; Banks and Hansen, 2002; Hansen, 2006). Within the central region, the orientation of the 2D bulk strain ellipse for early structures shows a slightly different orientation, but structures remain perpendicular to another. The 2D bulk strain ellipses for the southwestern and northeastern region are nearly opposite. The 2D bulk strain for intermediate- and long-wavelength folds remains unchanged, however during the formation of graben complexes the 2D bulk strain is oriented with maximum elongation oriented NE.

4.2.5. Window E - Geologic Relations and Relative timing

Window E (Plate 8), located in the southwestern region of the southern Tellus Regio map area (Figure 3), was selected for detailed mapping due to the preservation of ribbon, long- and short-wavelength fold terrain. This area is dominated by long, narrow basins that trend NE, and dissect the area into regions dominated by deformation and regions of low deformation within the basins. The basins lie within troughs created by long-wavelength folds. Long-wavelength folds are host to preserved structural fabric along their crests and limbs. The long-wavelength fold crests and NW region are host to pervasive tessera terrain, composed of narrowly spaced ribbons and orthogonal multiple-wavelength folds. Long-wavelength folds in the southeastern region of the window show wavelengths of ~20 km (Table 1), the crests and limbs of long-wavelength folds are host to orthogonal intermediate- (wavelengths of 6.5 km) and short-wavelength folds (wavelengths >1 km) and parallel the ribbon fabric throughout the window. Window E is host to different levels of flooded structural lows, ranging from large to small elongate basins and fill

within structural lows (most likely by lava fill). Units, fb_{c1} and fb_{c2}, both occupy the troughs of long-wavelength folds. Smaller, isolated basins, with unit fb_a, occur within structural lows of short-wavelength folds. Locally, wrinkle ridges and reactivated structures cut the fill in the larger basins. A distinctive suite of narrowly-spaced ribbon structures trends NE with general spacing of 1.54-2.2 km. A graben complex located in the north-central region of the window displays numerous east- and west- facing scarps. This complex is generally trending NNE and parallels ribbon fabric and long-wavelength folds.

The temporal relations of structural elements in window E (Plate 8) are characteristic of the larger southern Tellus map area, and provide an important tool to interpret the history of the area. NE-trending short-wavelength folds are widely distributed throughout the area. Orthogonal ribbons cut short-wavelength folds and locally short-wavelength folds continue onto ribbon ridges, indicating short-wavelength fold formation predated or possibly coincided with, ribbon formation. Ribbon structures are abundant throughout the area. Basin fill unit fb_a covers the troughs of both short-wavelength folds and ribbon structures, indicating the short-wavelength folds and the ribbon structures predated the emplacement of unit fba. Intermediate-wavelength folds, which occur throughout window E, generally trend NW and are host to parallel short-wavelength folds and orthogonal ribbons. Ribbon structures are interpreted as predating the formation of intermediate-wavelength folds, as discussed in section 3.4. Intermediate-wavelength fold troughs have not been covered by flood deposit material, highlighting preexisting structures across the intermediate-wavelength fold crests, limbs and troughs.

A suite of NE-trending long-wavelength folds are host to short-wavelength folds, ribbons, intermediate-wavelength folds and previous flood deposit material. The troughs of long-wavelength folds are covered by flood deposit material unit fb_{c1} and fb_{c2}. Burial of long-wavelength fold troughs occurred during or after formation of long-wavelength folds, and the troughs are in turn host to reactivated structures and few wrinkle ridges postdating flood material

deposition. A NE trending graben complex, parallel to long-wavelength folds, cuts across short-and intermediate-wavelength folds and ribbons, indicating that graben complexes formed late.

Window E preserves geometries and relative timing of structures that provide the tools for the interpretation of 2D Bulk strain. Early orthogonal ribbons and short-wavelength folds-relations are consistent with broadly synchronous formation and coherent bulk 2D strain (Plate 8) (Hansen and Willis, 1996 and 1998; Banks and Hansen, 2002; Hansen, 2006). The bulk strain associated with intermediate- and long-wavelength fold formation is different, although bulk 2D strain interpreted from short- and intermediate-wavelength folds is similar. However, during the late formation of graben complexes, the bulk strain changes orientation to oppose the long-wavelength fold bulk strain and aligns to match the bulk strain of intermediate-wavelength folds.

4.2.6. Window F - Geologic Relations and Relative timing

Window F (Plate 9), located in the southeastern region of the regional map area (Figure 3), was selected due to the presence of multiple wavelength folds and basins. Window F is dominated by three major basins, creating regions dominated by deformation and regions that lack deformation (in the basins). The basins are long, curvy and narrow, trending WNW to NW, and mark the troughs of long-wavelength folds. Long-wavelength folds are host to intermediate-, short-wavelength folds and ribbons. Basins are host to wrinkle ridges and a few pit chains.

Window F includes: long-wavelength folds, intermediate-wavelength folds, short-wavelength folds, ribbons, fault scarps and wrinkle ridges (Plate 9). Long-wavelength folds trending NW are host to parallel, WSW-trending intermediate-wavelength folds (wavelengths 8-13km; Table 1). A second suite of N-trending intermediate-wavelength folds is located in the NW region of the window; these folds trending at a high angle to long-wavelength, and previously mentioned, intermediate-wavelength folds. Generally, intermediate-wavelength folds host parallel short-wavelength folds with variations in wavelengths (0.7 km and 2 km). Short-wavelength folds are widely distributed throughout the area, trending N in the northern region, W

in the central region, and NE in the southern region of the map area. Window F hosts different

levels of flooded structural lows, ranging from the three major basins, to small filled basins

marking structural lows. The three large basins and their fill, units fb_{c1} and fb_{c2}, dominate window

F. Finger-like basins with fill units fb_b and fb_a occur in the troughs of intermediate- and short-

wavelength folds, and ribbons. Closely spaced SW-trending wrinkle ridges cut the fill in the in

large basins. A suite of narrowly-spaced, N-NNE-trending ribbon structures extends over the

eastern region of the window. Ribbon orientation is at high angles to adjacent long-, intermediate-

and short-wavelength fold crests. Fault scarps NW-trending cut across the area, most evident in

deformed areas but also present in basins. A suite of NE-trending pit chains cuts the western

region of the area.

The temporal relations of structural elements in window F (Plate 9) are characteristic of

the larger southern Tellus map area, and provide an important tool to interpret the history of the

area. Window F shows some of the most deformed terrain, although temporal relationships

appear to be similar throughout the area. Early short-wavelength folds record variations in trend

and wavelength (Table 1). The central short-wavelength folds show a slight increase in

wavelength, indicating that they may postdate very early short-wavelength folds (Table 1). This

juxtaposition of differently oriented structures of the same family indicates an early fluidity of the

surface. Ribbons cut short-wavelength folds, indicating that ribbons postdate early fold formation.

Both, short-wavelength folds and ribbons show flood deposit material (unit fb_a) in their respective

troughs, indicating that burial either coincided with or postdated early deformation. Intermediate-

wavelength folds topographically uplift (and down warp) parallel short-wavelength folds. Short-

wavelength folds, ribbon structures and early fill deposit material are preserved on the crests,

limbs and troughs of intermediate-wavelength folds, indicating that intermediate-wavelength fold

formation postdated these structures. Some intermediate-wavelength fold troughs are locally

buried by fill deposit material, unit fb_b, interpreted to postdate all preexisting structures.

Progressive deformation lead to the formation of NW-trending long-wavelength folds with little

variability in trend, recording more strength of the layer across the region at the time of long-wavelength fold formation. Long-wavelength folds crests are host to previously formed structures and local flood deposit material. The troughs of long-wavelength folds show extensive flood material and basin formation, units fb_{c1} and fb_{c2}, covering the majority of features present, indicating that long-wavelength fold formation postdated formation of short-, intermediate- and wavelength fold formation, ribbon and earlier basin formation, but predated the latest stage of flood material deposition. The formation of wrinkle ridges and fault scarps postdated basin formation, due to their crosscutting relationships. Fault scarps are interpreted to have formed late due to their near-constant orientation, which depicts a lack in the early structural fluidity of the area. I was unable to further determine the relative timing between those two structures due to their spatially separate position. Another suite of structures that are difficult to place temporally are three NE-trending pit chains. Pit chains crosscut units, fb_{c1} and fb_{c2}, postdating basin fill deposition but they are spatially separated from fault scarps and wrinkle ridges, which cut these same units.

Geometries and relative timing of structures in window F provide the tools for the interpretation of 2D bulk strain. Two regions within the map area record early near-opposite structural orientations, yet they preserve similar temporal relations. The regions appear to have been juxtaposed after their early deformation and later deformed as a coherent package. The central and north-western region each record early orthogonal ribbons and short wavelength folds-relations that are consistent with broadly synchronous formation, and coherent bulk 2D strain (Plate 9) (Hansen and Willis, 1996 and 1998; Banks and Hansen, 2002; Hansen, 2006). The 2D bulk strain for the central and north-western regions associated with short-wavelength fold and ribbons show a significant deviation in orientation to another. The 2D bulk strain associated with intermediate-wavelength folds in each region is similarly oriented to the 2D bulk strain interpreted from short-wavelength structures. The 2D bulk strain for long-wavelength folds across

the area is oriented similar to the orientation of central bulk strain, whereas the bulk strain for fault scarps is nearly opposite.

Geologic maps of the six detail windows place constraints on the geometric relationships and relative timing of structural elements across the southern Tellus Regio map area. In the following section I consider the results from each window in the regional context of southern Tellus Regio.

4.3. LAYER THICKNESS

Wavelength measurements from all six windows (Table 1) display a variety of contractional and extensional wavelengths for each structural suite. Early short-wavelength folds are followed by the formation of ribbon structures, which are in turn followed by intermediate-wavelength folds and finally long-wavelength folds and late graben complexes. Table 1 lists the wavelengths from across the study area. These structural wavelengths can be used in empirical calculations of layer thickness estimates at the time of structure formation; empirical ratios of 3 to 6 for contractional structures and 2 to 4 for extensional structures constrain the possible layer thickness estimates (e.g., Huddleston and Lan, 1995; Ghent and Tibulaec, 2002; Hansen, 2006; Table 1).

Estimate of layer thickness, and changes in layer thickness with time, are shown for each window of the southern Tellus Regio map area (Figure 6). The average layer thickness estimate for short-wavelength folds ranges from 0.1 to 1.15 km. Extensional ribbon structures record an overall layer thickness range of 0.76 to 1.33 km; these layer thicknesses broadly overlap the estimates for short-wavelength folds in the same areas. Intermediate-wavelength fold layer thickness estimates show two groups: 1.0 to 2.15 km, preserved in windows C, D and E; and 1.45 to 3.83 km thickness preserved in windows A, B, C and F. Window F also preserves evidence of a layer thickness of 2.3 to 4.6 km. Long-wavelength folds generally show a range of layer thickness of ~5 to 15 km.

All six windows record similar increases in layer thickness over time (Figure 6). The overlap between short-wavelength folds structures and ribbon structures, followed by intermediate- and long-wavelengths is consistent throughout all areas. The progression of structures based on layer thickness estimates is consistent with the broad structural temporal relationships interpreted across the entire plateau with short-wavelength structures forming early and long-wavelength structures forming later.

This scenario of an increasing layer thickness over time also places a strict requirement on the evolution of the rheological structure across the plateau (Hansen, 2006). The presence of a thin initial layer, with an increase of layer thickness over time, requires a sharp viscosity gradient with depth in order to form short-wavelength fold and ribbon structures (see discussion by Hansen, 2006). The surface must have been able to deform in a ductile and brittle fashion to form early short-wavelength contractional and extensional structures. Different strength of material in compression and tension enables the formation of ductile and brittle structures at the same time. In addition, the subsurface must have been host to low viscosity material, which would enable burial of structural lows by lava fill material. Continuous deformation and deposition of flood material would then increase the overall thickness and strength of the layer, resulting in progressively longer-wavelengths and graben formation.

4.4. HISTORY AND IMPLICATIONS

Geologic mapping of the southern Tellus Regio map area and the resulting interpreted history and implications are important to understand to evaluate the evolution of Tellus Regio as a crustal plateau. Summarizing all findings will allow the description of constraints that need to be considered for the evaluation of the existing models.

A general evolution arises from the geologic histories interpreted in each window. In general, contractional short-wavelength folds formed early, followed or accompanied with, ribbon structure formation; these structures formed on/in a thin (0.1-1.3 km thick) layer with a

sharp viscosity change at depth. Low-viscosity flood material locally flooded structural lows created by short-wavelength folds and ribbons. Fold formation and local flooding resulted in an increase in layer thickness. As the layer thickened, these early formed structures, and their respective basin fill, were uplifted (and down warped) by intermediate-wavelength fold formation. Troughs, limbs and crests of intermediate-wavelength folds preserve these previously formed structures. Commonly, regions of intermediate-wavelength fold troughs were then filled by more flood material, again resulting in a thickening of the layer. During formation of long-wavelength folds the previously deformed terrain was again uplifted (and down dropped). Troughs of late-formed long-wavelength folds were locally filled by flood material, which at this point experienced major flooding. During the latest stage of surface evolution graben complexes formed and overprinted all other structures; commonly, formation of graben complexes coincided with formation of similar trending fault scarps, parallel to the trend of the graben complex. Wrinkle ridges also occurred late, formed after the latest stage of basin flooding.

The temporal relations and spatial orientations of structures provide equally valuable information about the evolution of the surface, and possible mechanisms. The interpretation of the 2D bulk strain ellipses provide clues to how 2D bulk strain changed over time (Figure 7). During 'thin layer time' all six windows record different orientations of local 2D bulk strain (Figure 7, A-F), consistent with the interpretation that the early surface deformation recorded a high structural fluidity at a regional scale across the southern Tellus Regio map area. As the structural wavelengths increased with time, the result of increasing layer thickness, the fluidity of the surface deformation decreased, and the area deformed in a more coherent manner. By the time graben complexes form, two major 2D bulk strain domains remain, each marked by mutually perpendicular 2D bulk strain; one domain forms the southeastern part of southern Tellus Regio, the other domain comprises the rest of southern Tellus Regio.

Overall the orientations, spatial relations and temporal relationships of structural elements over the entire southern Tellus Regio map area record similar histories. They depict: 1)

46

that the layer thickness increased over time, allowing for short-wavelengths and ribbons to form early and then progressively increase wavelengths; 2) that deformation and flooding occurred broadly synchronous, preserving preexisting structures and thickening the layer over time; and 3) that 2D bulk surface strain changed over time, recording an early regional-scale fluidity that evolved to the layer behaving in a more coherent fashion.

This sequence of events calls for an high geothermal gradient over the entire regional map area that decrease over time. Even though the overall geothermal gradient decreased over time, it has to be initially high enough to allow for a sharp viscosity gradient beneath the initial thin layer, and to remain hot enough to allow low-viscosity material to fill structural lows. A high geothermal gradient would allow for an early thin layer enabling the formation of short-wavelength structures and progressive thickening of the layer by the addition of low-viscosity flood material. The high geothermal gradient allows for a sharp contrast in the BDT, which is needed to form the features recorded on Tellus Regio (Hansen, 2006; Ghent et. al., 2005; Ruiz et al., 2007). In addition, a high geothermal gradient would provide the surface with enough ductility to deform in a fluid-like manner across the plateau, which is evident in early 2D bulk strain ellipses. This fluidity in structural elements ceased as the geothermal gradient decreased and the layer thickness increased with time.

In summary, southern Tellus Regio is host to various structural elements and units that occur across the entire plateau. Fold wavelengths range from 0.7 km to >100 km and represent a progression of wavelengths from short-, intermediate-, to long-wavelength folds. Ribbon structures generally trend orthogonal to fold crests, although variability exists. Deposition of flood material occurred throughout the progressive deformation filling the troughs of all types of structural elements. Overall early structures display a fluid character that decreased with progressive deformation, and structures begin to form more coherent patterns. Collectively, the surface history records an increase in layer thickness with time. A high geothermal gradient with a sharp viscosity contrast at depth is required to form early short-wavelength folds and ribbons,

and a subsurface fluid likely formed the source of continuously available low-viscosity flood material. The relations documented here are consistent with relations documented for northern Ovda Regio (Hansen, 2006) although the current study area comprises a significantly larger area than that earlier study.

The history of the southern Tellus Regio map area and the resulting implications place critical constraints on hypothesis for crustal plateau formation. The next section will provide further constraints on model evaluation that have been previously discussed by other authors.

4.5 RESULTS OF PREVIOUS STUDIES

Tellus Regio has been the subject of localized studies focusing on the relative timing of magmatism and deformation within large intratessera basins (Banks, 2000; Banks and Hansen, 2000) and geologic mapping and modeling of the southwestern most region of Tellus Regio (Gilmore and Head 1995, 1996; Straley and Gilmore, 2007; Gilmore, 2009; Gilmore et al., 2010, 2011). This section summarizes the results of these previous studies.

Banks (2000) focused attention on three major intratessera basins on Tellus Regio, as exemplified in particular by relations in the so-called 'waffle basin' (Banks and Hansen, 2000). The results of Banks' study are in accordance with the results reported herein. The intratessera basins and surrounding areas are host to fold structures with multiple wavelengths ranging from ~1 km to >150 km and orthogonal ribbon structures with wavelengths ranging from 1-5 km; structural wavelength increased with time, and burial of structural lows with flood material accompanied deformation. Notably, these studies provided the first documentation of early flooding of the troughs of short-wavelength folds and ribbon structures, thereby providing some of the first evidence that a high geothermal environment accompanied the formation of Tellus Regio's structural features. These earlier results are comparable to the results of this study, and allow me to further use the intratessera basin results on the entire ribbon tessera terrain on southern Tellus Regio.

Gilmore and coworkers examined southwestern Tellus Regio and divided that region into several tectonic provinces including: an indenter, fold belt, crustal plateau interior, and western and SE marginal zones (Gilmore and Head 1995, 1996; Straley and Gilmore, 2007; Gilmore, 2009; Gilmore et al., 2010, 2011). Some of the results presented by Gilmore et al. (2010, 2011) are in accordance with this study. The presence of structural elements such as folds, ribbons, and graben complexes are similar to data presented herein; the description of structural elements, orientations and locations are supported by this study. For example, Gilmore and coworkers report fold wavelengths ranging from 3 to 45 km, similar to wavelengths reported in this study. However, this study also recognizes short-wavelength folds that generally range from 0.7 to 1.2 km, not previously reported by Gilmore and coworkers. In addition, this study provides data on basin development that indicates progressive deposition of flood material throughout progressive deformation of the surface.

Gilmore and coworkers interpreted southwestern Tellus Regio to have formed as separate domains that collided by indenter tectonics and were sutured along the fold belt domain. The western, SE, and interior domains, all part of the plateau, are comprised of preexisting fabrics. These three domains were further deformed as the indenter moved in and collided from the SW. As time progressed all domains were sutured together along the fold belt. This scenario could be viable, because certain fluidity within the domains is apparent; this fluidity later becomes more coherent as the region gained strength. However, results of the current study require that a thin layer, as evidence by the presence of short-wavelength folds, that progressively increases thickness over time occurred over the whole of southern Tellus Regio. The structural fluidity decreased over time and deformation became more coherent, independent of indenter type tectonics. Gilmore and coworkers also did not interpret that deformation was accompanied by deposition of flood deposit material. This study can address the different domains in the SW and more so across southern Tellus Regio, providing a detailed picture that indicates deformation of a large unit with fluidity across the terrain, rather than indenter type tectonics.

5. EVALUATIONS OF CRUSTAL PLATEAU FORMATION HYPOTHESES

In this section I evaluate the hypothesis for crustal plateau formation in light of the results and implications from geologic mapping of the southern Tellus Regio map area (Figure 1, Plate1, and Plate 2). The pulsating continents, mantle downwelling and mantle upwelling formation hypotheses are somewhat difficult to reconcile with the geologic evolution documented herein and the implications for southern Tellus Regio. On the contrary, the lava pond hypothesis and, and by association the bolide impact hypothesis, depicts an environment that creates similar surface deformation and evolution as documented for southern Tellus Regio.

5.1. PULSATING CONTINENTS

The pulsating continents hypothesis calls for thickening of crustal plateau terrain driven by cyclic compression and global subduction of tessera terrain (referred to by the hypothesis authors as similar to 'continental crust') (Romeo and Turcotte, 2008) (Plate 1, Figure 1). According to this hypothesis, initial compressional stresses within a low-density crustal area causes crustal thickening, which continues until an equilibrium between buoyancy forces is reached. After initial formation of contractional features and uplift of the plateau (the result of thickened 'continental crust'), the development of a gravitational instability causes radial graben and fractures to form, resulting in a widening and lowering of the plateau. Plateau collapse is followed by late-stage volcanic activity resulting in the burial of structural lows with flood lava material. This hypothesis predicts a progression of early-formed concentric contractional structures and late-formed radial extensional features, accompanied by burial of late-formed topographic lows; it further implies that the most important factor in plateau formation is the thickness ratio between crust and lithospheric mantle, a ratio of less than ~2:5 between crustal and lithospheric mantle thickness will result in compression and uplift of the crustal plateau, whereas a ratio above ~2:5 between crustal and lithospheric mantle thickness will cause the crust to spread out and collapse.

Although this hypothesis addresses the presence of early contractional structures in southern Tellus Regio, there are several factors that are contrary to hypothesis predictions. Early short-wavelength folds are accompanied, or followed immediately, by the formation of early extensional structures. A thin layer thickness with a sharp viscosity contrast at depth over thousands of square kilometers is required to do so. This rheological state cannot be accommodated in the pulsating continents hypothesis. Furthermore, the pulsating continents hypothesis does not accommodate a regionally extensive high geothermal gradient. In addition, there are relationships reported in this study that cannot be accommodated by the hypothesis including: 1) the near-equal spatial distribution of extensional features across southern Tellus Regio, and a general lack of evidence for radial extension; 2) the temporal evolution of the surface with orthogonal contractional and extensional structures forming broadly synchronous with deposition of low-viscosity flood material; 3) the fluid-like distribution of early-formed structures across the entire plateau; 4) a sharp contrast in viscosity with depth; 5) progressive increase in structural wavelengths with time; and 6) an increase of layer thickness over time.

5.2. MANTLE DOWNWELLING

The downwelling hypothesis calls for crustal accretion by sub-solidus flow or lithospheric accretion, caused by sinking of cold, dense lithosphere or by convective down flow within the mantle (Bindschadler and Parmentier, 1990; Bindschadler 1995; Bindschadler et al., 1992) (Plate 1; Figure 1). Downwelling in the mantle causes an initially downward flexure of the surface accompanied by the formation of radial contractional features. The regional crust begins to thicken with continuous formation of contractional features, forming the highest topography around the margins of the plateau, and marking regions of the thickest crust. Extensional features are created as the center of the thickened crust collapses under its own weight. The mantle downwelling hypothesis predicts: 1) the formation of early concentric contractional structures followed by later radial extensional features; 2) increase in crustal thickness followed by late

thinning of the crust and 3) a low geothermal gradient, which gets progressively colder with time and crustal thickening, and then increase with plateau collapse.

The mantle downwelling hypothesis could support the formation of contractional and extensional features similar to those observed in southern Tellus Regio and might even record the orthogonal character between but extensional and contractional structures; however, the regional spatial relations, nor the temporal relations predicted by the hypothesis, are consistent with regional spatial relations or temporal relations reported in this study. In addition, the formation of progressively longer-wavelength folds requires progressive thickening, which is not accommodated by this hypothesis. The downwelling hypothesis calls for a cold geothermal gradient as driving mechanism, contradicting the results reported in this study, which calls for a high geothermal gradient across southern Tellus Regio.

In addition, there are structural elements and relationships in southern Tellus Regio that cannot be accommodated by the mantle down welling hypothesis, including: 1) the fluid-like distribution of all structures across the plateau as recorded by 2D bulk strain ellipses; 2) the progressive increase in structural wavelength over time, with early short-wavelengths followed by progressively longer-wavelengths.

5.3. MANTLE UPWELLING

The mantle upwelling hypothesis calls for massive partial melting at shallow depths caused by a rising mantle plume or diffuse upwelling (Herrick and Phillips, 1992; Phillips and Hansen, 1998; Hansen and Willis, 1998; Ghent and Hansen, 1999; Hansen et al. 1999, 2000) (Plate 1). During the upwelling of the mantle plume, partial melting at the plume head occurs, and thermal energy from the plume mechanically anneals the crust and creates a rheological architecture with competent surface layer and a ductile substrate. The competent surface layer records progressive surface deformation as the layer thickens with time and progressive deformation. During uplift, caused by the plume head and lithosphere interaction, tensional

52

stresses result in ribbon fabric formation of the thin competent surface layer. Massive basalt flows are followed by magmatic underplating, both leading to an increase in layer thickness. Cooling and subsidence lead to local shortening and the formation of folds, with margin parallel folds along the margins and polyphase and/or domical interference folds in the plateau interior. Graben complexes form during late stages as a result of relaxation of folds. This hypothesis predicts a regional high geothermal gradient, a deformation history marked by the development of early extensional features followed by fold formation and late graben formation, and increase in competent layer thickness with increasing deformation.

Although this hypothesis predicts some features observed in southern Tellus Regio, including: 1) an increase in layer thickness with time; and 2) a high geothermal gradient, a few predictions only partially support the results from this study, or have caveats. The mantle upwelling hypothesis calls for a significantly higher geothermal gradient than either the pulsating continents or the downwelling hypotheses, however it does not predict, nor can it accommodate an exponential decrease in viscosity with depth as called for, based on the results of the current study. In addition, the mantle upwelling hypothesis formation of structure also somewhat matches what is observed on southern Tellus Regio, but does not, and cannot, address the formation of early-formed short-wavelength folds (see Hansen (2006) and Ghent et al. (2005) for further discussion).

In addition, the mantle upwelling hypothesis fails to accommodate: 1) the early formation of short-wavelength folds; 2) broadly synchronous formation of contractional and extensional structures and deposition of flood material; 3) the continuous increase of structural wavelength over time. Overall, the increase in layer thickness over time and presence of a high geothermal gradient alone does not provide sufficient evidence that this hypothesis is viable. For a complete discussion refer to Hansen (2006).

5.4. LAVA POND

The lava pond hypothesis calls for the progressive solidification and deformation of the surface layer of a huge lava pond, the formation of which is associated with the bolide impact hypothesis (Hansen, 2006). Massive amounts of partial melt, created by a large bolide that pierces a globally thin lithosphere and impacts the mantle, rises to the surface and forms a huge pond of lava. The so-called 'scum' of the lava pond evolves into the surface of an individual crustal plateau. At depth, in the upper portion of the ductile mantle, low-density mantle-melt residuum ultimately causes the region to uplift forming the topographic expression of the crustal plateau. Within the lava pond 'scum' early formation of short-wavelength folds is followed, or accompanied by, formation of orthogonal extensional structures; flood deposit material locally leaks to the surface filling local lows. Due to progressive deformation and flood material deposition, the 'scum' layer thickness increases with time. Longer-wavelength structures form successively, as the result of the deformation of a thicker layer. The buoyant melt residuum in the mantle causes isostatic uplift, leading to the rise and elevation of the plateau, during which time long-wavelength folds form. Two end-members scenarios are presented: a) the plateau remains uplifted if mantle-melt residuum remains in place as the lithosphere thickens due to secular cooling, or b) if mantle convection strips away the mantle-melt residuum, then the crustal plateau collapses, leaving the characteristic ribbon tessera terrain at low regional elevations, but relatively intact. Major predictions of this hypothesis for the surface evolution include: 1) a high geothermal gradient throughout deformation, 2) an increase in structural element wavelength and layer thickness over time, and 3) progressive orthogonal, extensional and contractional deformation accompanied by deposition of flood deposits over time.

This hypothesis accommodates the history and implications recorded on southern Tellus Regio. The lava pond and bolide formation hypothesis calls for an extremely high geothermal gradient that will create solid layer over a liquid layer within the crust; this rheological scenario allows for the formation of early short-wavelength folds and ribbon structures. A high geothermal

gradient is also predicted by the thermal modeling of ribbon structures (e.g., Gilmore et al, 2010, 2011, Ruiz, 2007). This geothermal gradient decreases over time, which is also consistent with the previously mentioned findings.

In addition, the structural features predicted within the context of the lava pond hypothesis are similar to those found in southern Tellus Regio. 1) The distribution of structural features across the plateau is explained by a huge lava pond and deforms the surface by convection within the lava pond. 2) Extensional and contractional structures broadly coincide with deposit of flood material. The extremely hot geothermal environment allows for lava to leak upward throughout the duration of deformation over the entire crustal plateau surface. 3) The fluid-like distribution of structures across the entire plateau could be accommodated by convective patterns within the lava pond, resulting in juxtaposition of different regional domains within Tellus Regio. 4) A decrease in geothermal gradient, combined with the progressive deformation and deposition of flood material across the surface aid in the formation of progressive wavelengths, similar to the structures observed on Tellus Regio. 5) The same factors also aid in thickening of the layer, which is necessary for formation of structures like those found on Tellus Regio.

The lava pond formation hypothesis provides a mechanism that, in context of southern Tellus Regio, not only depicts an accommodating view of the evolution of a crustal plateau by explaining the surface features, but also provides explanations for the implications arising out of the geologic history. The lava pond and bolide hypothesis is a plausible and reasonable formation hypothesis.

The geologic map of southern Tellus Regio provides a detailed picture of spatial distribution of structural elements that bear on the lava pond hypothesis (Plate 2). Fluid-like patterns of contractional and extensional structures are apparent across the map area. Coherent patterns can occur across certain regions, with structural element orientations and relations specific to that area. For example, window C (Plate 6), depicts an area that records juxtaposition

of two regions across a basin. The two regions are defined by early short-wavelength folds and ribbon structures, with later formed intermediate-wavelength folds. Both regions show similar geometric and temporal relations, although the structural orientation and 2D bulk strain of early structures are nearly opposing for the regions. These two regions are juxtaposed with one another on each side of the basin. However, late graben complexes cut across both regions with a similar NW trend, indicating that both regions deformed separately early on, but as time progressed, both sides fused together along the central basin to create one coherent region, and then deformed together as one. In context of the lava pond hypothesis, this early juxtaposition could stem from internal convection within the lava pond, which would allow the different regions of the thin scum on the surface to be rotated and juxtaposed with neighboring regions. But as time progressed and scum layer thickness increased, and earlier fluidity and mobility gave way to stiffer, less fluid, and less mobile, surface terrain, linking two previously juxtaposed areas into one.

This region, and others recorded in this study, are very similar to those interpreted by Gilmore et al. (2010, 2011) along the SW of Tellus Regio. The distinct domains proposed by Gilmore and coworkers could be also interpreted as different regions that developed locally due to convection within the lava pond; these regions would be later juxtaposed and ultimately sutured together to form a larger, more coherent region within the lava pond scum. In this scenario, the indenter proposed by Gilmore and coworkers would not have come from outside the plateau to collide with interior plateau terrains, but rather it would have formed as a stronger region along the margin of the Tellus Regio lava pond, which was moved by internal convection within the lava pond, colliding with other tracts of pond scum.

BIBLIOGRAPHY

Banks, B. K, 2000. Intratessera Flood-Lava Basins (ITBs) constrain timing of crustal plateau
        Structures, Tellus, Venus [Masters Thesis]: Dedman college, Southern Methodist
        University.

Banks, B. K. and Hansen, V. L., 2000. Relative timing of crustal plateau magmatism and
        tectonism at Tellus Regio, Venus: Journal of Geophysical Research, Vol. 105, no. E7, p.
        17,655-17,667.

Barsukov, V. L., et al., 1986. The geology and geomorphology of the Venus surface as revealed
        by the radar images obtained by Venera 15 and 16, Pro. Lunar Planet. Sci. Conf. 16th, Part
        2, J. Geophys. Res. Vol. 91, suppl., D378-D411.

Basilevsky, A. T., and J. W, Head, 1995. Global Stratigraphy of Venus: Analysis of a random
        sample of thirty six text areas: Earth, Moon, Planets, Vol. 66, p. 285-336.

Basilevsky, A. T., et al., 1986. Styles of tectonic deformations on Venus: Analysis of Venera 15
        and 16 data: Journal of Geophysical Research, vol. 91, D399-D411.

Basilevsky, A. T., and J. W. Head, III, 1998. The geologic history of Venus: A stratigraphic view
        Journal of Geophysical Research, Vol. 103, no. E4, p. 8531-8544.

Basilevsky, A. T., Head, James W.III, and Schaber, G. G., Strom1997, The resurfacing history of
        Venus: in Venus II: Geology, Geophysics, Atmosphere, and Solar Wind Environment:
        University of Arizona Press, p. 1047-1086.

Bindschadler, D. L. and M. E., Parmentier, 1990. Mantle Flow Tectonics: The Influence of a
        Ductile Lower Crust and Implications for the Formation of Topographic Uplands on
        Venus: Journal of Geophysical Research, Vol. 95, no. B13, p. 21,329-21,344.

Bindschadler, D. L., and J. W., Head, 1991, Tessera Terrain, Venus: Characterization and models for origin and evolution: Journal of Geophysical Research, 96, no. B4, p. 5889-5907.

Bindschadler D.L., and Tatsumura, M.J. 1992. Tellus Regio, Venus: Preliminary Magellan Observations of a region of Complex Ridged Terrain: Lunar and Planetary Sciences Conference XXIII, p. 103-104.

Bindschadler, D.L., Deharon, A. Beratan, K.K., Smrekar, S.S., Head, J. W., 1992. Magellan Observations of Alpha Regio: Implications for Formation of complex Ridged Terrains on Venus: Journal of Geophysical Research, Vol. 97, no. E8, p. 13,563-13,577.

Bindschadler, D. L., 1995. Magellan: A new view of Venus' geology and geophysics: Rev. Geophysics, Vol. 33, p. 459 – 467.

Conners, C., 1995. Determining heights and slopes of fault scarps and other surfaces on Venus using Magellan stereo radar: Journal of Geophysical Research, Vol. 100, no E7, p. 14361-14,381.

Farr, T. G., 1993. Radar Interactions with Geologic Surfaces: Guide to Magellan Image Interpretation: Jet Propulsion Laboratory Publication 93-24, p.47-57.

Ford, J. P., 1993. Magellan: The Mission and the System: Guide to Magellan Image Interpretation: Jet Propulsion Laboratory Publication 93-24, p.1-7.

Ford, J. P. and Plaut, Jeffrey, J., 1993. Magellan Image Data: Guide to Magellan Image Interpretation: Jet Propulsion Laboratory Publication 93-24, p.7-19.

Ghent, R. R. and Hansen, V. L., 1999. Structural and Kinematic Analysis of Eastern Ovda Regio, Venus: Implications for Crustal Plateau Formation: Icarus, v. 139, p. 116-136.

Ghent, R. R., and I. M. Tibulaec, 2002. Ribbon spacing in Venusian tessera: Implications for layer thickness and thermal state: Geophysical Research Letters, Vol. 29, no. 20, p. 61-1 – 61-4.

Ghent, R. R., Phillips, R. J., Hansen, V, L., and D. C. Nunes, 2005. Finite element modeling of short-wavelength folding on Venus: Implications for the plume hypothesis for crustal plateau formation: Journal of Geophysical Research, Vol. 110, E11006.

Gilmore, M. S. 2009. Tellus Regio, Venus: Evidence of tectonic assembly of tessera terrain and implications for exploration: Lunar and Planetary Science Conference, 40th Annual Meeting, no. 2015.

Gilmore, M. S., and J. W. Head, 1995. Formation of Tessera Terrain on Venus: A structural Analysis of Tellus Regio: Lunar and Planetary Science Conference, 26th Annual Meeting, p.461-462.

Gilmore, M. S., and J. W. Head, 1996. Evidence for Collisional Tectonics at Tellus Regio Tessera, Venus: Lunar and Planetary Science Conference, 27th Annual Meeting, p.415-416.

Gilmore, M.S., et al., 2010. Mapping and Modeling of Tessera Collision Zone, Tellus Regio, Venus: Lunar and Planetary Science Conference, 40th Annual Meeting, no. 1769.

Gilmore, M.S., et al., 2011. Constraints on Tessera Composition from Modeling of Tellus Regio, Venus: Lunar and Planetary Science Conference, 41st Annual Meeting, no. 2053.

Grimm, R. E., 1994. The Deep Structure of Venusian Plateau Highlands: Icarus, Vol. 112, p. 89-103.

Hansen, V. L., 2006. Geologic constraints on crustal plateau surface histories, Venus: The lava pond and bolide impact hypothesis: Journal of Geophysical Research, Vol. 111, E110110.

Hansen, V., L., and J. J. Willis, 1996. Structural Analysis of a Sampling of Tesserae: Implications for Venus Geodynamics: Icarus, v. 123, p. 296-312.

Hansen, V. L., and J. J. Willis, 1998. Ribbon Terrain Formation, Southwestern Fortuna Tessera, Venus: Implications for Lithosphere Evolution: Icarus, Vol. 132, p. 321-343.

Hansen, V. L., Banks, B. K., and R. R. Ghent, 1999. Tessera Terrain and crustal plateaus, Venus: Geology, V. 27, p. 1071 – 1074.

Hansen, V. L., Phillips, R. J., Willis, J. J. and R. R. Ghent, 2000. Structures in tessera terrain: Issues and Answers: Journal of Geophysical Research, Vol. 105, p. 4135-4152.

Herrick, and Phillips 1992, Geological correlations with the interior density structure of Venus: Journal of Geophysical Research, Vol. 97, p. 16,017-16,034.

Huddleston, P., and L. Lan, 1995. Rheological information from geological structures: Pure Appl. Geophysics, Vol. 145, p. 607-620.

International Astronomical Union (IAU). Gazetteer of Planetary Nomenclature, Planetary Names: Venus, Tellus Tessera. (http://planetarynames.wr.usgs.gov/Feature/5909, last accessed 4/23)

Kirk, R. L., Soderblom, L. A., Lee, E. M., 1992. Enhanced Visualization for Interpretation of Magellan Radar Data: Supplement to the Magellan Special Issue: Journal of Geophysical Research, Vol. 97, no E10, p. 16,371-16,380.

Mackwell, S.J., Zimmerman, M.E., Kohlstedt, D.L., 1998. High temperature deformation of dry

    diabase with application to tectonics on Venus: Journal of Geophysical Research, Vol.

    102, p. 975–984.

Plaut, Jeffrey, J., 1993. Stereo Imaging: Guide to Magellan Image Interpretation: Jet Propulsion

    Laboratory Publication 93-24, p. 33-45.

Romeo, I., and Turcotte, D.L., 2008. Pulsating continents on Venus: An explanation for crustal

    plateaus and tessera terrains: Earth and Planetary Science Letters, Vol. 276, p. 85-97.

Phillips, Roger R. and Hansen, Vicki L., 1994. Tectonic and Magmatic Evolution of Venus:

    Annual Review Earth and Planetary Science, Vol. 22, p. 597 -654.

Phillips, R. J. and Hansen, V. L., 1998. Geological Evolution of Venus: Rises, Plains, Plumes,

    and Plateaus: Science, Vol. 279, p. 1492-1497.

Ruiz, J., 2007. The heat flow during the formation of ribbon terrains on Venus: Planetary and

    Space Science, Vol. 55, p 2063-2070.

Senske, D.A., 2010. Tessera Terrain on Venus: Comparing Phoebe Regio and Tellus Tessera:

    Lunar and Planetary Science Conference, 41st Annual Meeting, no. 1256.

Senske, D.A. and Plaut, J.J., 2009. Geologic Evidence for a thick volcanic crust in part of Tellus

    Tessera, Venus: Lunar and Planetary Science Conference, 40th Annual Meeting, no. 1707.

Slonecker, A.J. and Hansen, V.L., 2012. Preliminary Structural and Geologic Mapping of

    Northern Tellus Regio, Venus: Abstract 2012 Annual Planetary Geologic Mappers

    Meeting, Flagstaff, AZ.

Snyder, D., 2002. Cooling of lava flows on Venus: The coupling of radiative and convective heat

    transfer: Journal of Geophysical Research, Vol. 107, no E10, p. 101 – 108.

Stofan, E. R., Senske, D. A., Michaels, G, 1993. Tectonic features in Magellan Data: Guide to

      Magellan Image Interpretation: Jet Propulsion Laboratory Publication 93-24, p.47-57.

Straley, B.L., and Gilmore, M. S., 2007. Mapping and Structural Analysis of SW Tellus Regio,

      Venus: Lunar and Planetary Science Conference, 48th Annual Meeting, no. 1657.

Tanaka, K. L., et al. (1994), The Venus Geologic Mappers' Handbook, 2nd Ed., U.S. Geological

      Survey. Open File Rep., 94-438, 52 pp.

Tanaka, K. L., Senske, D.A., Schaber, G.G., and M. Price., 1995. The geologic framework of

      Venus: Venus II Abstract booklet, pp 47.

Tanaka, K. L. et al., 2010. Planetary structural Mapping: Planetary Tectonics, Cambridge

      University Press, New York, p. 351-396.

Weitz, C. M., 1993. Impact Craters: Guide to Magellan Image Interpretation: Jet Propulsion

      Laboratory Publication 93-24, p. 75-93.

Zimbelman, James R., 1999. Image Resolution and evaluation of genetic hypothesis for planetary

      landscapes: Geomorphology, Vol. 37, p. 179-199.

Table 1. Summary of structural wavelengths collected for windows A-F and regional measurements for southern Tellus Regio and corresponding layer thickness estimates.

	Lineament type	Trend	Latitude N	Longitude E	Transect Length km	# of lineament	Spacing km	Short-λ folds 6:1, km	Short-λ folds 3:1, km	Intermediate-λ folds 6:1, km	Intermediate-λ folds 3:1, km	Long-λ folds 6:1, km	Long-λ folds 3:1, km	Extension fabric 4:1, km	Extension fabric 2:1, km
A	short-λ folds	W/E	41.75	86.75	52	71	0.73	0.12	0.24						
	short-λ folds	W/E	42.5	85.5	10	13	0.77	0.13	0.26						
	intermediate-λ folds	W/E	42.5	85.5	22	3	8.00			1.33	2.67				
	intermediate-λ folds	W/E	41.75	86.25	52	6	8.70			1.45	2.90				
	intermediate-λ folds	NW	42.25	87.25	36	4	9.00			1.50	3.00				
	ribbon structures	NWN	41.75	86	37.5	18	2.08							0.52	1.04
	ribbon structures	NWN	42	85.75	20	13	1.53							0.38	0.77
	ribbon structures	NWN	42.25	85.75	18.4	8	2.30							0.58	1.15
	wrinkle ridges	WSW	42.5	86.5	20	17	0.85								
	wrinkle ridges	WSW	42	85	15	18	1.20								
B	short-λ folds	W/E	39.25	82	29.5	29	1.02	0.17	0.34						
	short-λ folds	W/E	39.5	81.5	16	22	0.73	0.12	0.24						
	short-λ folds	NW	39.75	82.5	38	31	1.23	0.20	0.41						
	intermediate-λ folds	NW	39.75	81.75	56	6	9.33			1.56	3.11				
	intermediate-λ folds	NW	39.5	82	56	5	11.20			1.87	3.73				
	ribbon structures	N/S	38.5	81.25	31.5	15	2.10							0.53	1.05
	ribbon structures	N/S	39.5	82	24	9	2.67							0.67	1.33
C															
west	short-λ folds	NW	38.5	72.5	34.5	51	0.68	0.11	0.23						
	short-λ folds	NW	38.25	73.5	38.5	36	1.07	0.18	0.36						
	intermediate	NW	38.5	73	68	7	9.71			1.62	3.24				
	ribbon structures	N	38.5	74.25	46	24	1.92							0.48	0.96
east	short	NE	37.5	75	33	39	0.85	0.14	0.28						
	short	NNE	38	76.25	18.5	24	0.77	0.13	0.26						
	short	NE	38.75	76	15.5	23	0.67	0.11	0.22						
	intermediate	NE	37.75	76	36	6	6.00			1.00	2.00				
	intermediate	NE	37.25	75.5	46	4	11.50			1.92	3.83				
	ribbons	NW	37.5	76	26	13	2.00							0.50	1.00

63

Table 1. Summary of structural wavelengths collected for windows A-F and regional measurements for southern Tellus Regio and corresponding layer thickness estimates.

	lineament type	Trend	Latitude N	Longitude E	Transect Length km	# of lineame	Spacing km	short-λ folds 6:1km	short-λ folds 3:1 km	intermediate-λ folds 6:1km	intermediate-λ folds 3:1 km	long-λ folds 6:1km	long-λ folds 3:1 km	extension fabric 4:1 km	extension fabric 2:1km
D	short-λ folds	NE	31.25	78.25	71.5	51	1.40	0.23	0.47						
	short-λ folds	W/E	32.25	79	28.5	14	2.04	0.34	0.68						
	short-λ folds	WNW	31.25	77.5	34.5	10	3.45	0.58	1.15						
	intermediate	NW	31.5	79	65	11	5.91			0.99	1.97				
	long-λ folds	NW	32	78.5	111	3	37.00					6.17	12.33		
	ribbons	NE	32	78	108	41	2.63							0.66	1.32
NE	ribbons	NNE	32.25	79	35	17	2.06							0.51	1.03
SW	ribbons	NNE	31.25	77.5	15.5	7	2.21							0.55	1.11
	graben	NW	32	78											
	wrinkle ridges	SE	31.25	79.25	29	13	2.23								
E	short-λ folds	NW	29.5	77	56	59	0.95	0.16	0.32						
	short-λ folds	NW	29.25	76.75	17	19	0.89	0.15	0.30						
	short-λ folds	NW	30.25	77.25			0.87	0.15	0.29						
	intermediate-λ folds	NW	29.5	77.5	32.5	5	6.50			1.08	2.17				
	long-λ folds	NE	29	77.5	82	4	20.50					3.42	6.83		
	extension (ribbs)	NE	29.75	76.75	65	30	2.17							0.54	1.09
	extension (ribbs)	NE	29.5	77.5	18.5	12	1.54							0.39	0.77
	graben	NE	30	77											
F	short-λ folds	W/E	30.75	81.75	59.5	29	2.05	0.34	0.68						
	short-λ folds	NW	30.25	82.25	20	27	0.74	0.12	0.25						
	intermediate-λ folds	W/E	30.75	81.5	55.5	4	13.88			2.31	4.63				
	intermediate-λ folds	N/S	31.25	81	43.5	5	8.70			1.45	2.90				
	ribbons	NE	31	82	53	22	2.41							0.60	1.20
	fault scarps	NW	31	81	42	20	2.10							0.53	1.05
	fault scarps	NW	30.25	81	25	17	1.47							0.37	0.74
	wrinkle ridges	SE	31.25	82	37.5	23	1.63								

Table 1. Summary of structural wavelengths collected for windows A-F and regional measurements for southern Tellus Regio and corresponding layer thickness estimates.

	lineament type	Trend	Latitude N	Longitude E	Transect Length km	# of lineame	Spacing km	short-λ folds 6:1km	short-λ folds 3:1 km	intermediate-λ folds 6:1km	intermediate-λ folds 3:1 km	long-λ folds 6:1km	long-λ folds 3:1 km	extension fabric 4:1 km	extension fabric 2:1km
STR	intermediate	NW	37.5	79	191	14	13.64			2.27	4.55				
	intermediate	NW	38.75	72.5	137.5	9	15.28			2.55	5.09				
	long-λ folds	NE	36	88	175	5	35.00					5.83	11.67		
	long-λ folds	NW	34	79	225	7	32.14					5.36	10.71		
	long-λ folds		29	82	150	4	37.50					6.25	12.50		
minimum								0.11	0.22	0.99	1.97	3.42	6.83	0.38	0.77
maximum								0.58	1.15	2.31	4.63	6.25	12.50	0.67	1.33
average								0.20	0.40	1.53	3.06	4.79	9.58	0.52	1.04
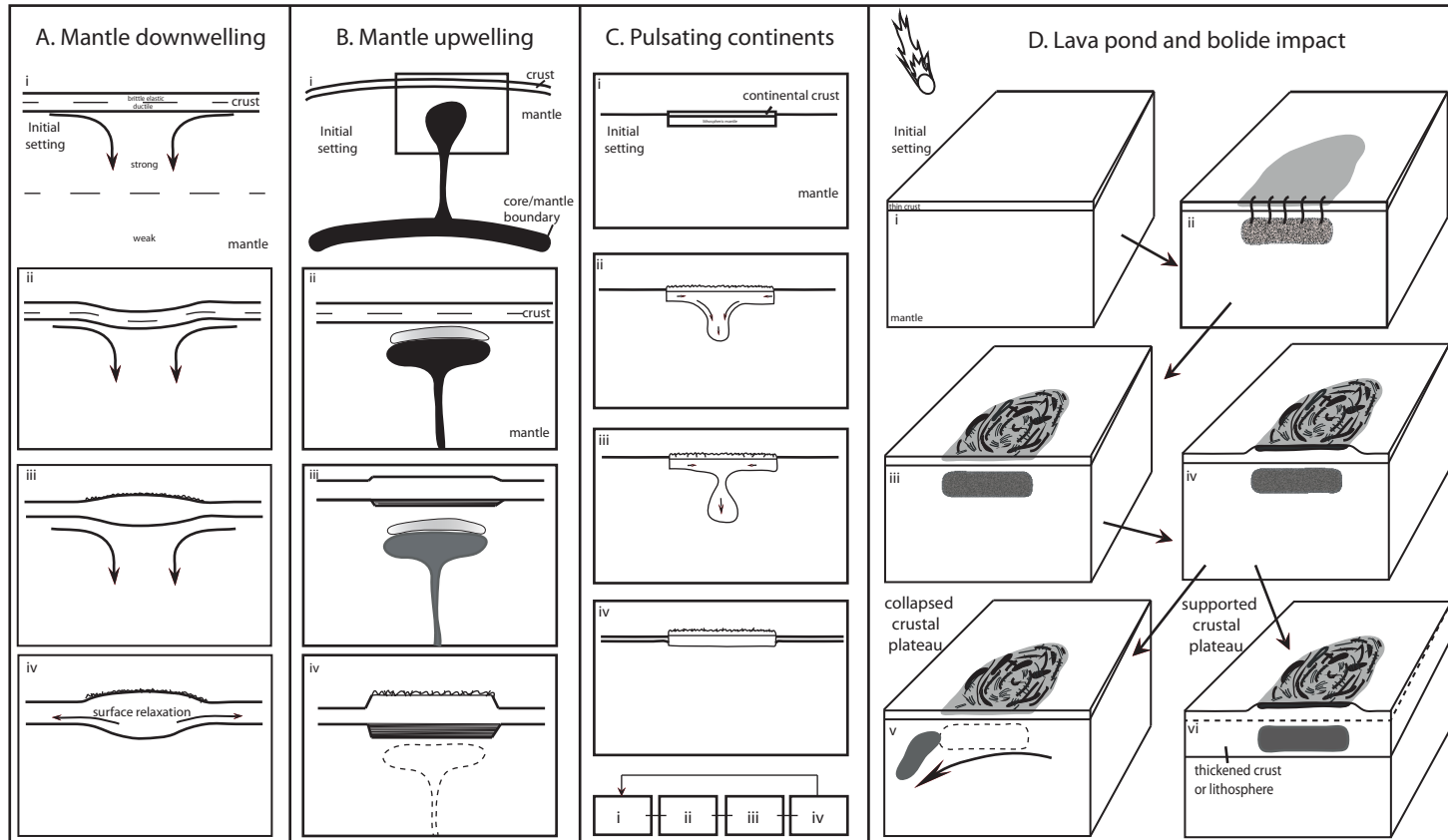
Figure 1. Cartoon model of crustal plateau formation hypotheses. Each column highlights major deformation stages (i-vi) for each hypothesis. Mantle downwelling (A) is initiated by sinking of denser material and thickening of overlying crust. The stages highlight the initial setting and sinking of dense lithosphere (i), downward flexure of the deformation surface (ii), thickening and deformation of the surface (iii), and late stage relaxation (iv). Mantle upwelling (B) is caused by an upwelling mantle plume and underplating. Stage I indicates the upwelling of a mantle plume, followed by partial melting at the plume head (ii) and surface deformation and thicking of the crust (iii), and late stage deformation (iv). The pulsating continents hypothesis (C) calls for cyclic deformation of the crust initiated by density differences. The stages (i-iv) describe, respectively, early compression, the development of a gravitational instability accompanied by deformation and the late stage volcanism and relaxation. The cyclic nature of this hypothesis is described below stage iv. The lava pond and bolide impact hypothesis (D) calls on a bolide impact to create partial melt in the mantle and deforms the surface during progressive solidification. The stages describe the intial setting with impeding impact of a bolide(i), the creation of massive partial melt leaking to the surface (ii), the formation of early structures and flooding (iii) and progressive thickening of the deforming layer. Two end members are presented: v indicates the mantle melt residuum being swept away, resulting in the collapse of the crustal plateau, and vi indicates secular cooling of the lithosphere, resulting in a supported crustal plateau. See text and plate 1 for further discussion.
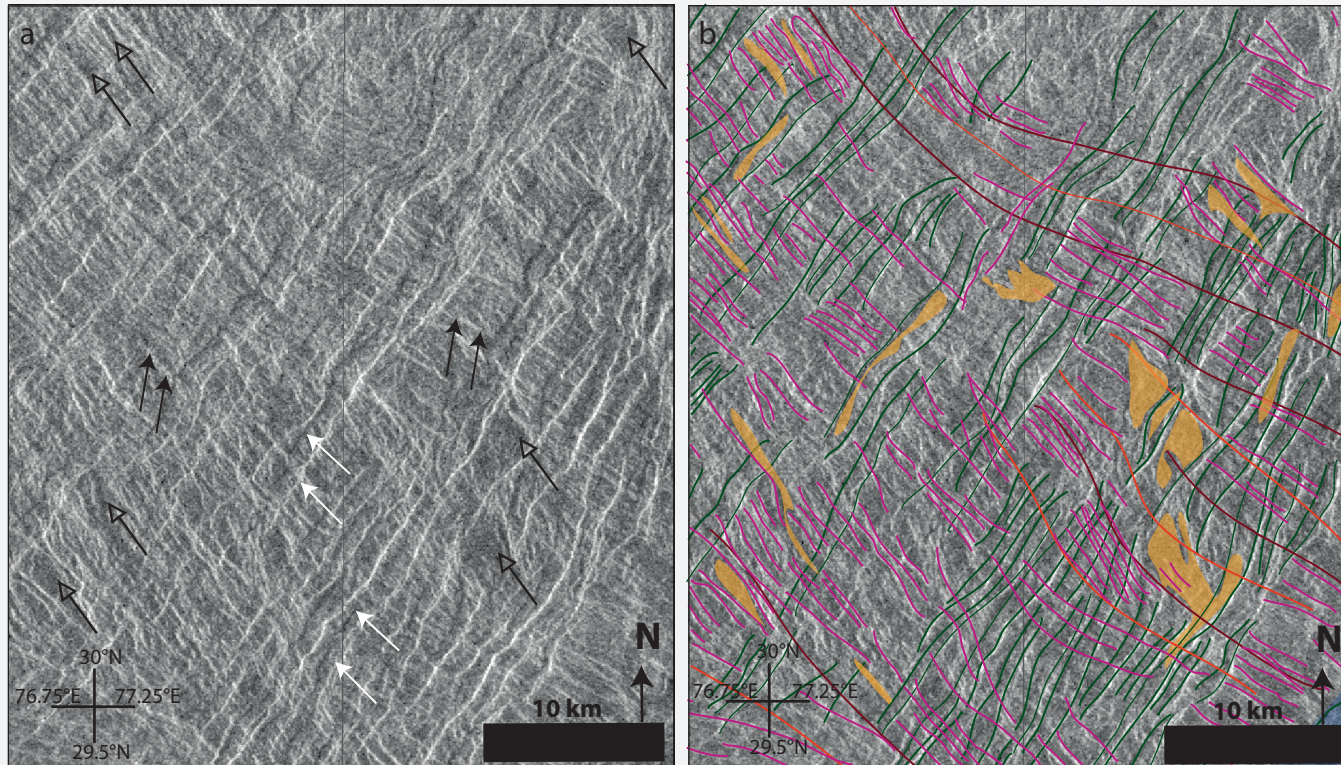
Figure 2. Left-look SAR image (a) and geologic map (b) depicting different types of lineaments. (a) Black arrows indicate lineaments with gradual change in slope, interpreted as short-wavelength folds. White arrows indicate dark lineaments followed by bright lineament, indicating a ribbon structure trough. Open-headed arrows indicate burial by low-viscosity fill material. (b) The corresponding geologic map highlights ribbons and short- and intermediate-wavelength folds, with flooding in troughs of short-wavelength folds and ribbons. Intermediate-wavelength folds were interpreted using stereo images. See text for discussion.

Map Key

Structures

── intermediate-wavelength (troughs)
── intermediate-wavelength (crests)

── short-wavelength (crests)

── ribbons troughs (light lineaments)
── ribbons dark (dark lineaments)

Material Units
flood basins

fb_a
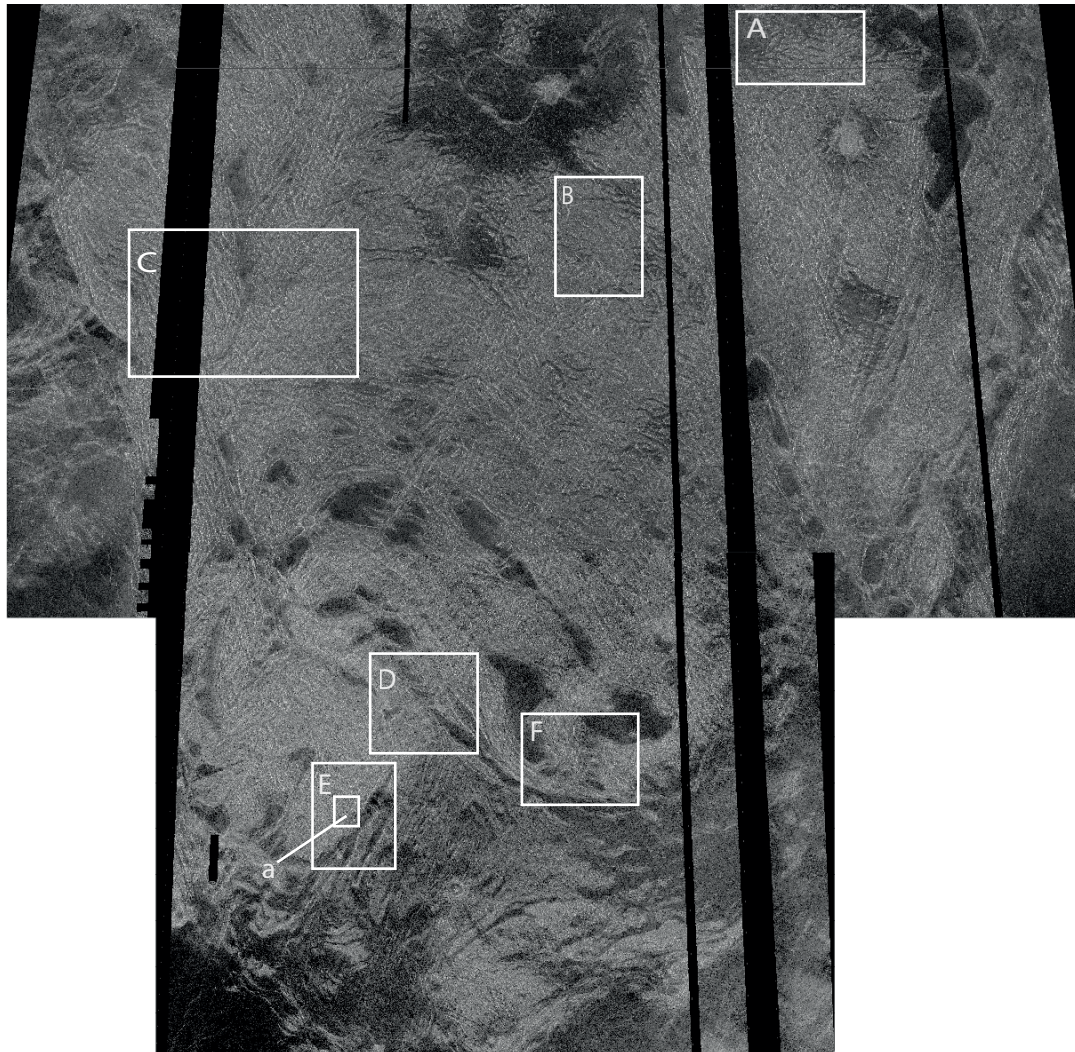
Figure 3. Left-look SAR with window locations across southern Tellus Regio. (a) Indicates the location of Figure 2.
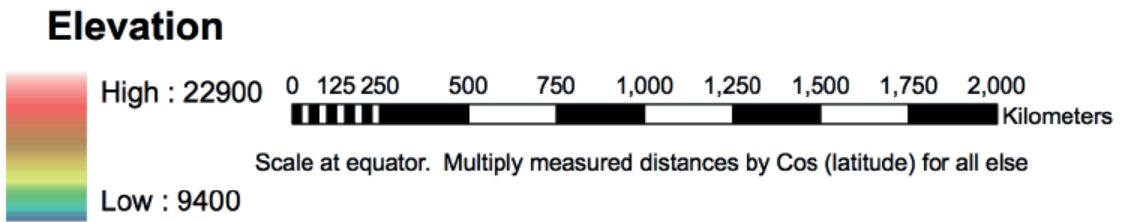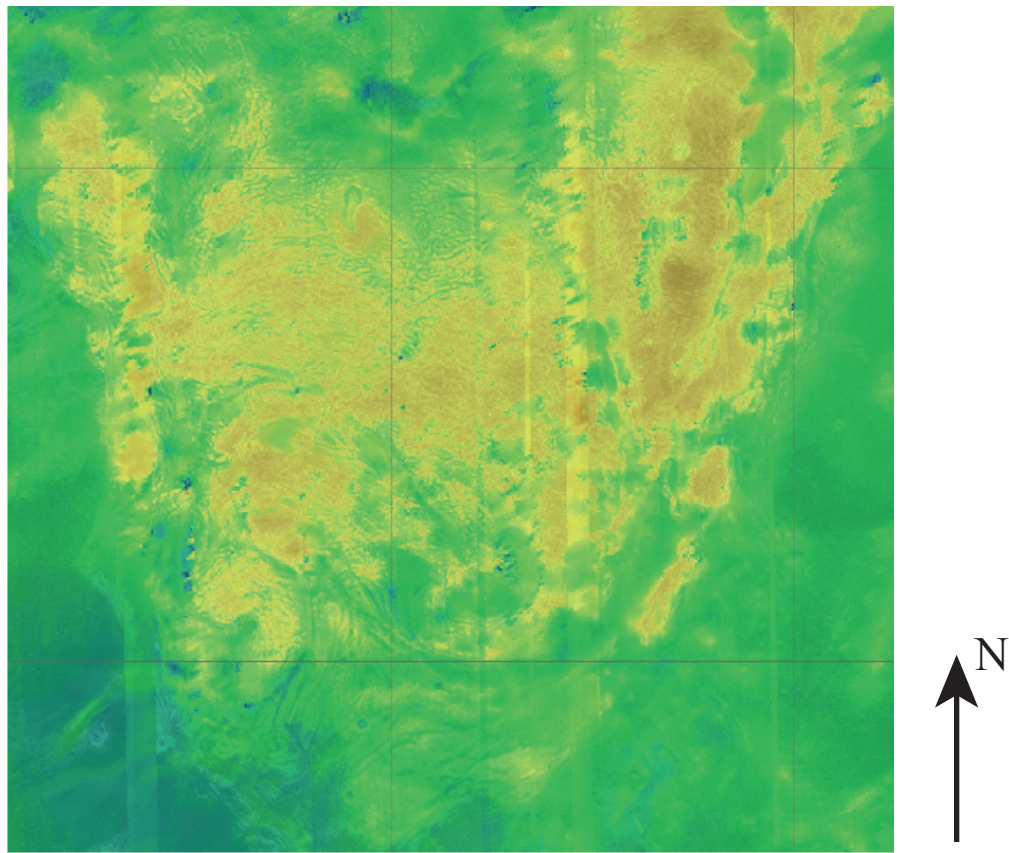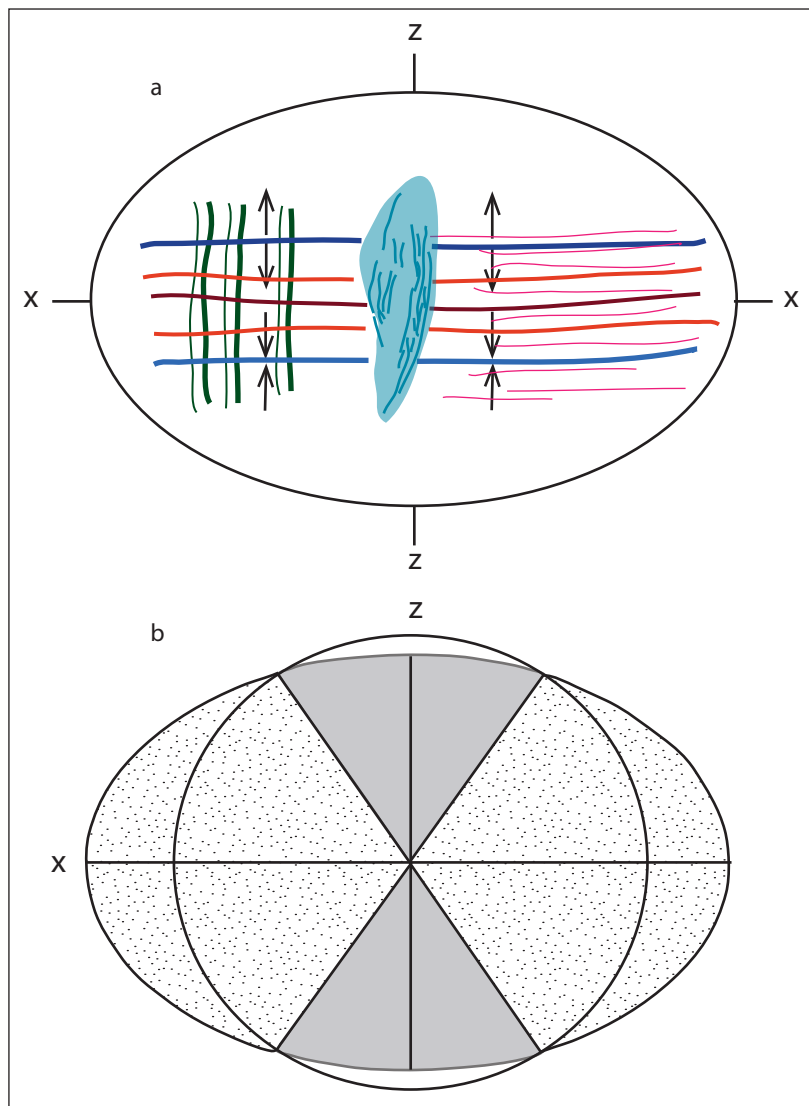
Figure 4. Stereo-derived topography data showing high and low elevations across the plateau. Note the generally similar elevation across southern Tellus Regio (from Herrick et.al, 1993).

Map Key

Structures

long-wavelength (troughs)	
long-wavelength (crests)	
intermediate-wavelength (troughs)	
intermediate-wavelength (crests)	
short-wavelength (crests)	

shear fracture

ribbons troughs (light lineaments)
ribbons dark (dark lineaments)

faults scarps in graben complex
graben basin

Figure 5. (a) Family of structures that can form synchronously or within the same bulk strain (map view). (b) Finite strain ellipse illustrates regions of finite shortening (light gray), and finite elongation (stippled pattern). Principal strain axes are x maximum elongation and z minimum elongation (after Hansen and Willis, 1996).
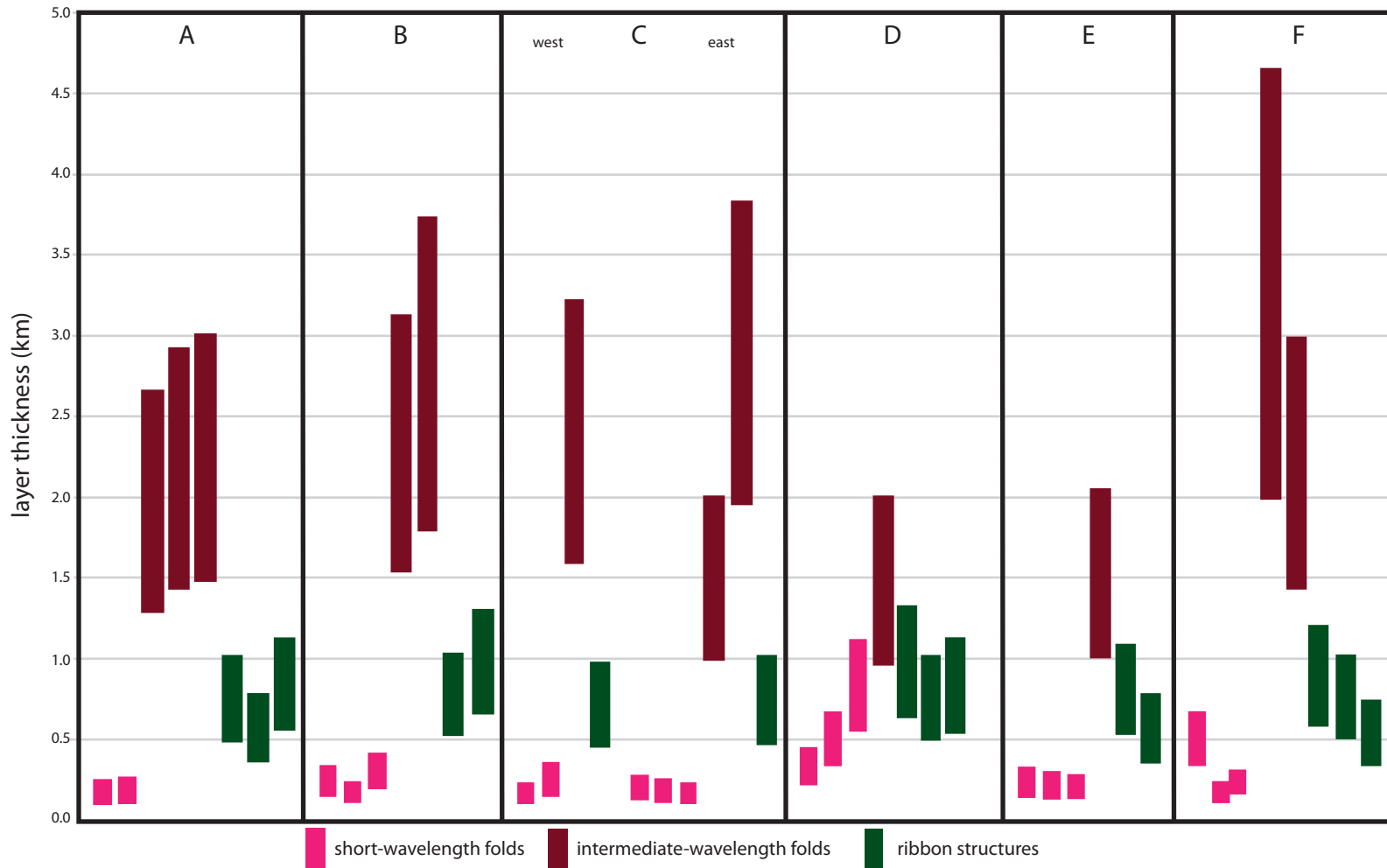
Figure 6. Plot of layer thickness associated with short-, and intermediate-wavelength folds and ribbon structures from each of the windows (data in Table 1).
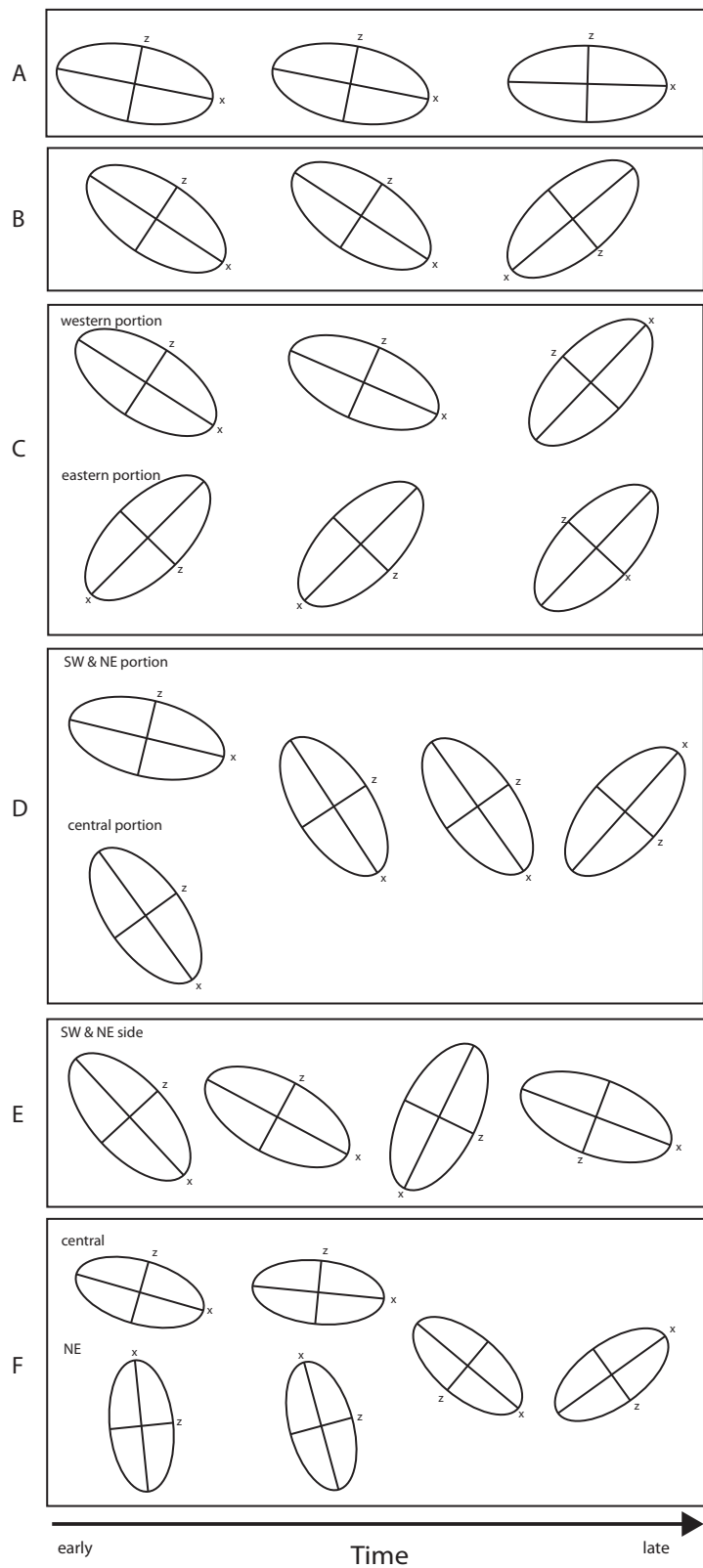
Figure 7. Composite of all 2D bulk strains for each window. A-F mark the windows, generally showing early variability in 2D bulk strain, apparent in changing structural element orientation. Through time, this variability in structural orientation ceases and the areas deform in a more coherent fashion. 2D bulk strain during late-stage formation only shows little variation across the map area.

72